



UNIVERSIDAD NACIONAL DE COLOMBIA

Estimation of the relative biological effectiveness of heavy ions using the dose-mean transfer energy

Adriana Marcela Forero Torres

National University of Colombia
Science Faculty, Physics Department
Bogota, Colombia
2019

Estimation of the relative biological effectiveness of heavy ions using the dose-mean transfer energy

Adriana Marcela Forero Torres

In Partial Fulfillment of the Requirements for the Degree
Master in Medical Physics

Director:

Doctor in Physics, Mario Antonio Bernal Rodriguez

Codirector:

Doctor of Medical Physics, Maria Cristina Plazas De Pinzón

Line of Research:

Microdosimetry

Research group:

Medical Radiation Physics, Unicamp

National University of Colombia
Science Faculty, Physics Department
Bogota, Colombia
2019

This copy corresponds to the document endorsed by us to be presented to the jury committee

Director
Mario A. Bernal

Codirector
Maria Cristina Plazas

Dedicated to each woman who decided to take
this fantastic way of science

Acknowledgements

To my parents and brother, who have been a great support in every project I undertake.

To my friend, David Esteban Suárez, an exceptional partner in this way of physics and for his help through difficult times.

Special thanks to Professor Mario Bernal for giving me the opportunity to delve into this fascinating area of microdosimetry and for his important contributions to the realization of this thesis.

To the Professor María Cristina Plazas for her support in each of my crazy projects.

I have to thank the State University of Campinas for the opportunity to be there as a special student for a month and having allowed me to use all the resources available, from a computer cluster, office, libraries, and others. All these items were essential for the completion of this thesis.

Abstract

Ionizing radiations induce damages in DNA when interacting with living beings. These damages may lead to biological effects such as chromosome aberrations and cell death. The radiation potential for inducing DNA damages is related to the capacity of radiation to produce densely ionization patterns in the irradiated tissues. This capacity is often related to the linear energy transfer (LET); however, this quantity is not enough for determining the relative biological effectiveness (RBE) of a given radiation quality. For instance, two heavy charged particles (ions) with the same LET show different RBE. So far, researchers have used the dose-mean lineal energy as a quantity to estimate the RBE of ionizing radiations. In this work, we explore a new microdosimetric quantity called dose-mean energy transfer. We also implemented a computational tool for the calculation of such variables using Geant4-DNA toolkit. In addition, a comparison with another classical microdosimetric variable known as dose-mean linear energy was made and RBE variable was determined for each of them. The results show consistent values between dose-mean linear energy and the proposed new microdosimetric variable dose-mean transfer energy. Finally, based on the results obtained for the RBE of each of the variables, the impact of the new variable on the RBE estimation was studied.

Key words: LET, RBE, Geant4-DNA, dose-mean lineal energy, dose-mean transfer energy.

Resumen

Las radiaciones ionizantes inducen daños en el ADN cuando interactúan con los seres vivos. Esos daños pueden dar lugar a efectos como las aberraciones cromosómicas y la muerte celular. El potencial de la radiación para inducir ese tipo de daños está relacionado a la capacidad de la radiación para producir un denso patrón de ionizaciones en los tejidos irradiados. Esta capacidad es relacionada a la transferencia de energía lineal (LET). Sin embargo, esta cantidad no es suficiente para determinar la efectividad biológica relativa (EBR) de una calidad de radiación determinada. Hasta el momento, muchos investigadores han usado al dose-mean lineal energy como una cantidad para estimar el RBE de radiaciones ionizantes. En este trabajo, nosotros exploramos una nueva grandeza microdosimétrica llamada dose-mean transfer energy. También se implementó la herramienta computacional para el cálculo de dicha variable haciendo uso de las librerías de Geant4-DNA. Adicionalmente, se ha realizado una comparación con la variable dose-mean linear energy y la nueva variable microdosimétrica dose-mean transfer energy. Finalmente, basados en los resultados del RBE obtenidos para cada una de las dos grandezas, se estudió el impacto de la nueva en la estimación del RBE.

Palabras claves: LET, RBE, Geant4-DNA, dose-mean linear energy, dose-mean transfer energy.

Index of Figures

- 2-1 Representation of ionizations and excitations produced by a charged particle impacting on an atomic target. 7
- 2-2 Range of protons in water [NIST] 8
- 2-3 Total stopping power for protons on water [NIST]. 9
- 2-4 Comparison of the X-ray depth dose curve with the SOBP used in passive proton beam delivery for clinical treatment 11
- 2-5 Representation of the effect of different types of radiation on DNA: low LET, high LET and extremely high LET. 13
- 2-6 Arrangement and scale of the bases of DNA, chromosomes, nucleosomes, and chromatin fibers. 14
- 2-7 Deposition of energy in microscopic volumes. 14
- 2-8 Fano’s theorem allows to replace a micrometer volume with another larger volume with a lowest density where a particle does the same deposition of energy. 19
- 2-9 Schematic representation of different parts of Linear-Quadratic Model . . . 20
- 2-10 Typical survival fraction of cell irradiated with a heavy ions (red continuous line) and other radiation of reference as photons (blue dotted line) 22
- 2-11 RBE as a function of the LET. The example depicts a 10% clonogenic cell survival as the biological endpoint 24
- 2-12 RBE as a function of the LET with shouldered $\alpha/\beta = 1-4 Gy$. In this figure the nomenclature is p: red; He: blue; C: gray; Ne: orange; ions heavier than Ne: green 25

- 3-1 Measurement histogram to the nearest meter, to the nearest centimeter and the limit to a continuous function 30
- 3-2 Inverse method 31
- 3-3 Rejection and acceptance method 32
- 3-4 Structure of geant4 38
- 3-5 Excitation energies of liquid water used in Geant4-DNA, obtained by empirical fit of optical data 41
- 3-6 Total ionization cross sections for electrons obtained by different models. . 41

3-7	Total cross sections of ionizations process for protons and helium atoms in water obtained from Rudd model (energies below 500 keV and from Born model (energies above 500 keV)	43
4-1	Example of electron and photon entering the scoring volume for describing a difference between energy transfer and imparted energy	46
4-2	Incident radiation impacting the scoring volume to illustrate difference between kerma and absorbed dose	47
4-3	Sampling to obtain the microdosimetric variables. In red the positions of the different depositions. One deposition is chosen randomly for each track and at a distance of not less than r the center of the sphere will do the sampling and then an $f(y)$ is defined according to the number of depositions that fall within of sphere. The total number of depositions (red points) are 14 and inside of sphere fall 3 depositions, for this reason $f(y) = \frac{3}{14}$	48
4-4	Simulation geometry. It consist of a world with a box shape and filled with liquid water. There is also a logical smaller volume with box shape.	50
4-5	Process included in G4DNAPhysics constructor for electrons	51
4-6	Process included in G4DNAPhysics constructor for protons	51
4-7	Geometry used to find a mathematical expressions to determine if a point is inside a cylinder.	53
4-8	Model to calculate transfer energy	54
4-9	Secondary electron spectrum ($\text{keV}^{-1}\text{photon}^{-1}$) corresponding to liquid water irradiated with ^{60}Co photons. It was used as input for determining microdosimetric variables for the reference quality.	56
5-1	Dose-mean lineal energy y_d obtained from sampling a spheres and cylinders of similar dimensions.	60
5-2	Comparison between y_d values obtained by author with geant4 toolkit and values obtained by Chen, for a spherical region of $d = 1\mu\text{m}$	61
5-3	Comparison between y_d values obtained by author with geant4 toolkit and y_d values obtained by for a cilindrical region of $d = 10\text{nm}$, equal diameters and lengths.	62
5-4	Distribution of y_d for spherical sampling with radius 2 nm and energy equal to 1 MeV	63
5-5	Distribution of t_d for spherical sampling with radius 2 nm and energy equal to 1 MeV	63
5-6	Comparison between y_d and t_d for spherical sampling with radius 2nm . . .	65
5-7	Comparison between y_d and t_d for spherical sites with radius of 10 nm . . .	65

5-8	Comparison between y_d and t_d for spherical sites with radius of 30 nm . . .	66
5-9	Comparison between y_d and t_d for spherical sites with radius of 5 μm . . .	66
5-10	RBE determined for a spherical sampling volume with 2 nm radius for both microdosimetric quantities.	69
5-11	RBE determined for spherical a sampling volume with 10 nm radius for both microdosimetric quantities.	69
5-12	RBE determined for a spherical sampling volume with 30 nm radius for both microdosimetric quantities.	70
5-13	RBE determined for a spherical sampling volume with 5 μm radius for both microdosimetric quantities.	70
5-14	Graph obtained for comparison of RBEs obtained by author with diameter 30nm and the data values of experimental measurements of RBE	71

Index

Acknowledgements	vii
Abstract	ix
0.1 Objectives	2
0.1.1 General Objective	2
0.1.2 Specifics Objectives	2
1 Introduction	3
2 Interaction of charged particles with matter	5
2.1 Generation of field around the projectile	5
2.2 Excitations and ionizations produced by charged particles	6
2.3 LET	6
2.4 Range	7
2.5 Multiple elastic scattering	8
2.6 Multiple inelastic scattering	9
2.7 Heavy ion therapy	11
2.8 Heavy ions radiobiology	12
2.9 Microdosimetry	13
2.9.1 Experimental microdosimetry	19
2.10 The Linear-Quadratic model	19
2.11 Relative Biological Effectiveness	21
2.12 RBE models	22
2.12.1 RBE Measurements	23
2.12.2 Animal models	24
2.12.3 Clinical models	25
3 The Monte Carlo methods in microdosimetry	29
3.1 Fundamentals of the method	30
3.1.1 Probability theory	30
3.1.2 Sampling theory	31

3.1.3	Random number generator	33
3.1.4	Monte Carlo Method in radiation transport	34
3.1.5	Monte Carlo Uncertainties	34
3.2	Monte Carlo Codes	36
3.2.1	EGS	36
3.2.2	FLUKA	36
3.2.3	MCNP	37
3.2.4	PENLOPE	37
3.2.5	ETRAN	37
3.2.6	Geant4	37
3.2.7	Geant4-DNA project	40
3.3	Geant4 physics models for microdosimetry and nanodosimetry	40
3.3.1	Inelastic models for electrons	40
3.4	Inelastic models for protons	42
4	Method	45
4.1	The Model	47
4.2	Organization of the user code	49
4.2.1	Description of the geometry	49
4.2.2	Description to physics List	49
4.2.3	Description of the primary source	50
4.2.4	Description to Tracker class and sampling	52
4.2.5	Determination of lineal energy and transfer energy	53
4.3	Determination of microdosimetric variables for reference photons	55
4.3.1	Processing with ROOT	55
5	Results	59
5.1	Dose-mean lineal energy in different sampling structures	59
5.2	Validation of microz for protons microdosimetry	60
5.3	Probability Density Function of microdosimetric variables	62
5.4	Calculation of protons microdosimetric variables	64
5.5	Photons microdosimetric variables	64
5.6	RBE calculation	67
6	Conclusions	72

0.1 Objectives

0.1.1 General Objective

Create a new microdosimetric variable that allow a better description of relative biological effectiveness for energetic ions with computational models

0.1.2 Specifics Objectives

Propose a function shape for a new microdosimetric variable called dose mean transfer energy that allow us understand phenomena and mechanisms which entails to better relative biological effectiveness of ions with regard photons.

Elaborate computational tools to allow us determinate microdosimetric spectra of the already established microdosimetric variables as dose mean linear energy and the new microdosimetric variable dose mean energy transfer.

Determinate of RBE by both microdosimetric variables proposes for performing an evaluation of physical processes that explain the sensibility of this factor for energetic ions with same LET.

1 Introduction

Along the last century, radiotherapy treatment has involved sophisticated techniques using photon external beams produced from linear accelerators for clinical applications. Different techniques have been implemented, such as IMRT (Intensity Modulated Radiotherapy), VMAT (Volumetric Modulated Radiotherapy) and SRT (Stereotactic Radiotherapy). These forms of Radiotherapy are based on CT-image reconstruction of patients. By and large, these techniques allow to deliver dose to target volumes with an accuracy of 3–5 %. However, these techniques in many cases, deliver high doses to healthy tissues [1].

Currently, other Radiotherapy techniques using heavy charged particles are used, such as protons and carbon ions, which present different energy distributions both at micro and macroscopic scales, when compared with photon beams. At macroscopic scale, they show a fast increase of energy deposition near to Bragg peak [2]. At microscopic scale, individual particles deposit their energy along the particle trajectory, producing clusters of ionization and/or electronic excitations. These clusters induce complex damages in the DNA cells, which are more difficult to repair by the cellular mechanisms, leading to higher Relative Biological Effectiveness (RBE) than that observed with photon and electron beams. RBE is used to quantify of the capacity of certain radiation quality for inducing some biological damage relative to that of a reference radiation, commonly ^{60}Co or 220 kVp X-rays [3].

Traditionally, two approximations have been followed to estimate RBE: experimental and computational. The former is based on the irradiation of cell cultures and the quantification of the damage according to a given biological endpoint. The latter uses biophysical models that can be implemented in a computer, commonly based on the use of Monte Carlo simulations of radiation transport. The irradiation of cell cultures implies that experimental conditions are far from those found in clinical conditions. However, this technique represents the Golden Rule in Radiobiology. Nevertheless, due to systematic dependencies it has not been possible to obtain high resolution measurement of RBE in terms of LET in-vitro systems and this approach presents very high uncertainties associated to radiobiological quantities [4].

Biophysical modelling of the radiation-tissue interaction and its biological response allows a more flexible study where several parameters can be manipulated along a wider spectrum than that observed under restricted experimental conditions. Some of these models are the MKM (Microdosimetric Kinetic Model) and LEM (Local Effect Microdosimetric) [5–7], which can fairly predict the RBE of heavy charged particle beams. Assuming a geometry for the target and considering particle track structures, both models can translate a given response of a biological systems to photon beams to that observed on heavy charged particles.

In this thesis a new microdosimetric variable called dose-mean transfer energy is introduced. In addition, the capacity of this quantity to estimate the RBE of proton beams is explored, comparing it to the well-known dose-mean lineal energy. A computational tool for the calculation of this variable was developed. If this quantity allows the RBE estimation in a successful way, it could represent a change of paradigm in the microdosimetry and Radiobiology. Maybe models developed from the 70's should be reevaluated since they are based on the deposited energy rather than on the energy transfer. This thesis contains five chapters. In chapter 1, some important physical and biological models for the transport of heavy particles description are reviewed. Chapter 2 treats the theory of the Monte Carlo method in radiation transport, including different codes developed for this problem. In Chapter 3, the computational model for the calculation of the two microdosimetric variables mentioned above and their corresponding RBE, is described. In Chapter 4, the results of this work will be shown in detail. In chapter 5, the author will describe the ideas and suggestions for future developments of this work.

2 Interaction of charged particles with matter

The interaction of radiation with matter is a stochastic process since it is not possible to deterministically find the value of the main quantities involved in that process. That is, the energy lost during a collision, the distance travel between successive interactions, the scattering angle, and so many others. In the context of macrodosimetry some quantities can be determined in a non-stochastic fashion, mainly through the expectation value of stochastic quantities. This is the case of the absorbed dose, which can be defined as the expected value of the specific energy.

In the case of photon radiation, non-stochastic variables, such as the dose, are considered acceptable given the low energy fluctuations per cell. In the case of heavy charged particles, imparted energy fluctuations are very large because energy depositions are densely concentrated close to the primary particle track. Thus, these particles are more efficient for inducing biological effects. These statistical fluctuations were studied by Rossi [8], where a set of 150 cells were exposed to different types of radiations with less than 1 MeV for photons and more than 1 MeV for fission neutrons. There, they found that the mean free path of neutrons was comparable to the cell dimensions. The irradiation with photons showed low imparted energy fluctuations per cell, while for neutrons such fluctuations were considerably higher, where 98% of the cells did not have any energy deposition and the others received energies that were 50 times larger than the average. In this sense, heavy particles demand the use of new approximations accounting for the stochastic nature of radiation-matter interaction, and this is precisely what microdosimetry does. So in this new approach, a new stochastic quantity and its corresponding dose-mean value are defined.

2.1 Generation of field around the projectile

Charged particles generate an electromagnetic field around them. This field mediates the interaction with the atomic or molecular target system. This includes atomic electrons and

nuclei. For relativistic projectiles, there is a magnetic component, besides the electrostatic one. The water molecule is the main target in biological tissues. In the course of the interaction of charged particles with a condensed medium such as liquid water, we can use the dielectric response function [9,10]. When the interaction occurs, the electric field \vec{E} depends on time and position and generates an electric displacement \vec{D} , which can be expressed as

$$\vec{D} = \epsilon \cdot \vec{E}. \quad (2-1)$$

By applying the Fourier decomposition to \vec{D} and to \vec{E} , the response function can be expressed as a complex coefficient

$$\epsilon(E, K) = \epsilon_1(E, K) + i\epsilon_2(E, K). \quad (2-2)$$

According to the first Born approximation [10], the probability of energy and momentum transfer E and $\hbar K$, respectively, is proportional to the imaginary part of inverse of the dielectric response function

$$Im[-1/\epsilon_2(E, K)]. \quad (2-3)$$

This dielectric formalism allows accounting for condensed phase effects in a natural way.

2.2 Excitations and ionizations produced by charged particles

The principal mechanism for the interaction of charged particles with matter is the coulombian interaction. Charged particles interact mostly with atomic electrons of the medium, losing energy through processes such as excitations and ionizations. In excitations, as is shown in the Fig. **2-1**, a charged particle interacts with the atom, which is electronically excited to a higher energy state. If the energy transfer is high enough, the electron may be removed from the atom, leaving the latter ionized. There can also be a coulombian interaction with the whole atom during which the state of the atom remains unchanged, which is just an elastic scattering. Electrons lose little energy during this kind of scattering due to their small mass relative to that of the target. Yet, a heavy charged particle may lose a large fraction of its energy when the target mass is similar to the projectile one.

2.3 LET

The concept LET is closely related to the electronic stopping power. In fact, it is also called restricted stopping power, which means that energy transferred to electrons above

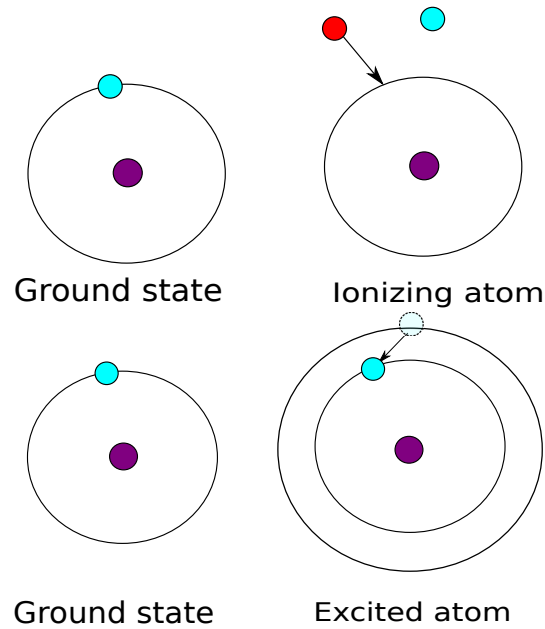


Fig. 2-1: Representation of ionizations and excitations produced by a charged particle impacting on an atomic target.

certain threshold is not accounted for. The reason to introduce such a threshold is to have a measure of locally deposited energy, in the vicinity of the primary particle track, since according to the current understanding, this local energy deposition has a strong influence on the biological effect induction. Higher energy deposits may result in ionization electrons that have high enough energies to escape from the spot, thus carrying away energy to more distant regions irrelevant for the local biological effect.

A mathematical definition of LET is the quotient of dE by dx , dE is the expected value of the energy transfer to secondary electrons along the path dx , due to collisions with energy transfers lower than the threshold mentioned before (Δ).

$$LET_{\Delta} = \left(\frac{dE}{dx} \right)_{\Delta} \quad (2-4)$$

2.4 Range

The range of a charged particle in an absorber provides a measure of its energy. The particle loses energy primarily by the excitation and ionization of atoms along its path. These energy losses occur as a large number of small increments. Heavy ions have such

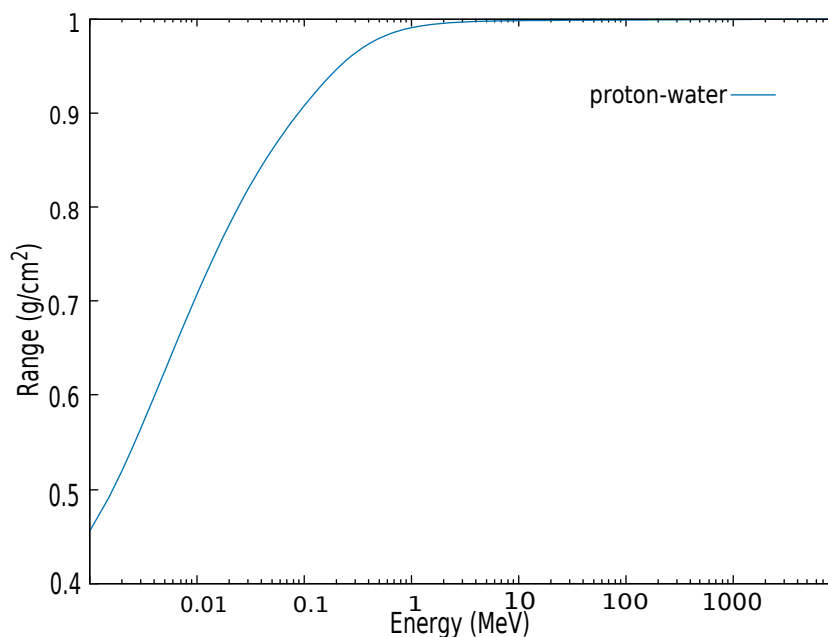


Fig. 2-2: Range of protons in water [NIST]

a large momentum that their direction is not changed appreciably during the slowing process. Eventually, they lose all their kinetic energy and come to rest. The expected value of the penetration of the particle into medium is called range, and depends on the charge and speed of the particle, and the mass density and chemical composition of the medium. Slow heavy charged particles lose more energy per unit path length than fast particles. This effect can be observed in the ionization along the path of particles; the number of ions produced per unit distance is small at the beginning of the path, rises to a maximum near the end of the path which is called the Bragg peak, and then falls sharply to zero when the particle becomes too slow to produce any further ionization (the range end point).

2.5 Multiple elastic scattering

A charged particle traveling through matter is deflected by many small-angle scatterings. These deflections are due to coulomb scattering from the atoms; thus it is called Coulomb scattering. Although scattering angles are small, a great number of collisions contribute to this effect and make it appreciable. This process was studied in detail by Moliere [11] and it is characterized by a Gaussian dependence on the scattering angle

$$\theta = \frac{13.6 \text{ MeV}}{\beta_c p} z \sqrt{\frac{x \rho_x}{X_0}} \left[1 + 0.038 \cdot \ln \left(\frac{x \rho_x}{X_0} \right) \right] \quad (2-5)$$

where β_c is the particle speed, p is the momentum, and ρ_x is the mass thickness of the material and X_0 is the thickness of material. The polar scattering angle is denoted as θ . The expected number of particles N scattered along θ after having travelled a thickness x that can be estimated as

$$\frac{dN}{d\Omega} = \frac{1}{2\pi\theta_0^2} \exp\left(-\frac{\theta^2}{2\theta_0^2}\right), \quad (2-6)$$

where θ_0^2 is the variance of the scattering angle, also known as angular straggling. Of course, there are other models for elastic scattering but they will not be treated here.

2.6 Multiple inelastic scattering

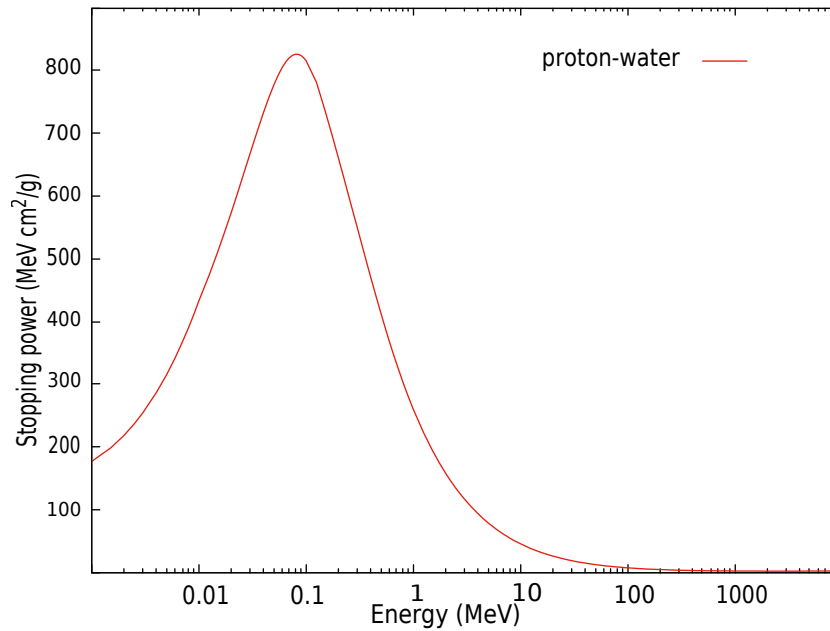


Fig. 2-3: Total stopping power for protons on water [NIST].

The stopping power is the expected value of the energy lost by a particle per unit path length. It is only defined for charged particles as

$$S = \left\langle \frac{dE}{dx} \right\rangle, \quad (2-7)$$

where dE is the energy lost by the particle along the path length dx . It is commonly measured in units of $(\text{keV}/\mu\text{m})$ and depends on the density of the medium. However, it is commonly tabulated divided by the density of the medium, which is just the mass stopping power S/ρ . This latter quantity does not depend on the phase state of the material (up to a good approximation). It can be seen as the expected value of the energy lost by the particle per unit mass thickness $(\text{MeV}\cdot\text{cm}^2/\text{g})$. In general, the stopping power can be classified according to the process involved, namely electronic, radiative, and nuclear

$$S_{total} = S_{electronic} + S_{radiative} + S_{nuclear}. \quad (2-8)$$

Electronic processes include excitation and ionization, while radiative losses are mainly due to Bremsstrahlung. Nuclear stopping is due to elastic scattering by the whole atom. For light particles, such as electrons and positrons, electronic and radiative processes are dominant. For heavy charged particles, only electronic and nuclear components are considered, at least for not relativistic particles.

Consider a projectile (ion) with kinetic energy E_o that impacts on a given material. During the penetration into the medium, it slows down gradually until it stops, being implanted as a strange atom inside the material. In the course, it undergoes slight angular deviations due to electronic processes when its speed is high, and more notable deviations by the nuclear stopping at relatively low speeds. Due to its random nature, the trajectory is intricate and unique. We denote as $R[\text{cm}]$ the total path length along the trajectory, from the point of incidence until it comes down to rest. The greater the incident energy E_o , the greater the path length. This range is also known as the Continuous Slowing Down Approximation Range, or CDSA range. It can be defined as follows:

$$R(E_0) = \int_{E_0}^0 S^{-1} dE \quad (2-9)$$

Bethe developed a successful theory based on the first Born approximation and obtained the following for the mass stopping power

$$(S/\rho) = 4\pi N_A r_e^2 m_e c^2 \frac{Z}{A} \frac{z^2}{\beta^2} \left[\ln \frac{2m_e c^2 \beta^2 \gamma^2}{I} - \beta^2 - \frac{\delta}{2} \right] \quad (2-10)$$

where N_A is the Avogadro number, r_e is the classical electron radius, Z and A are the atomic number and mass number of the target atom, respectively, I is the mean excitation energy of the target, and δ is the density effect correction. The behavior of the stopping power for protons in water is shown in Fig. **2-3**, where its dependence on the projectile energy can be observed [12].

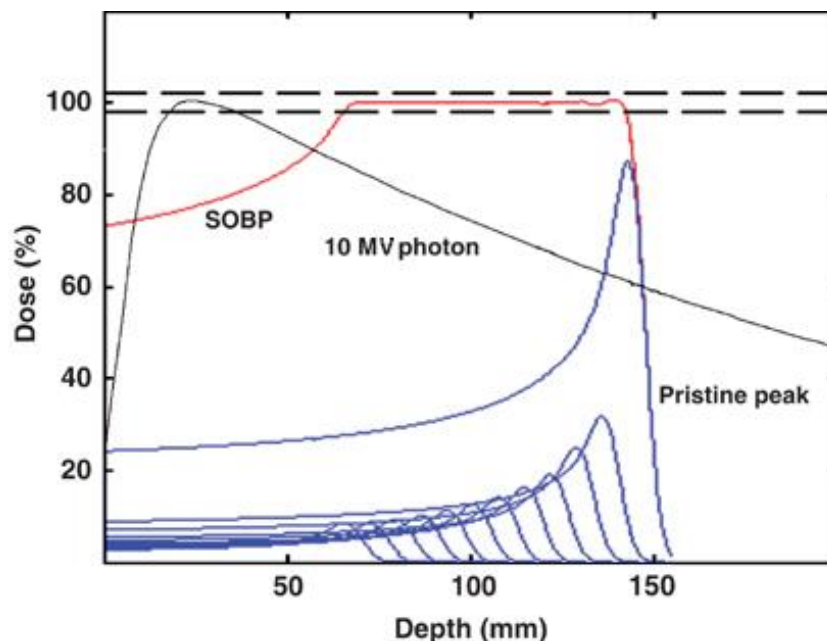


Fig. 2-4: Comparison of the X-ray depth dose curve with the SOBP used in passive proton beam delivery for clinical treatment

2.7 Heavy ion therapy

Presently one of the major health risks mankind faces is cancer. One in three people will suffer from this disease or side effects of its treatment at some stage in their life. Because of the deleterious effects that cancer and often current treatment forms are having on the human population, better treatment techniques are constantly being sought. Besides surgery, external beam radiation therapy is a mainstay of cancer treatment and cure. High energy protons and hadrons such as carbon ions are an important innovation in external beam radiation therapy, providing highly conformal dose distributions, thus sparing normal tissues through the benefits afforded by the Bragg peak.

The use of fast protons as a clinical tool was first suggested by Wilson in 1946 and was first used clinically in 1954. Since its inception, there have been many advances in areas including accelerators development, focussing technologies and treatment planning. A typical proton therapy department is based around a single accelerator with multiple treatment rooms making it more complex and expensive than X-ray therapy which exists as “stand alone” modules. Proton delivery techniques can be categorized as passive or active in the delivery of a uniform dose to the treatment volume. Passive techniques, which have been most commonly used in the clinical setting spread the beam laterally

using a combination of gold and Lexan foils . The combination of two materials, one of low and the other of high atomic number produces a flat beam of constant flux and a constant range. Typically a dual scattering foil arrangement is utilized; that is optimized to deliver a flat field of the cross sectional area required for treatment. The beam is then modulated in depth using a rotating plastic wheel that effectively allows for the superposition of multiple Bragg peaks of varying intensity to create a region of uniform high dose called the Spread-Out Bragg Peak (SOBP) [13]. The beam is then collimated by brass or Cerrobend apertures and its penetration depth is varied by means of a wax bolus. Such an arrangement creates a uniform dose across the treatment volume as displayed in Fig. 2-4.

2.8 Heavy ions radiobiology

The DNA molecule is the main target in the interaction of radiation with cells. To inactivate a cell, the DNA has to be damaged severely so the cell can not be reproduced. The DNA molecule contains all the genetic information necessary for the cell function and reproduction. This molecule is polymer composed of two chains arranged into a double helix. Each of these chains is a succession of nucleotides. The double helix is wound around the histones, which join to form the nucleosome. All these are compacted to form the 30nm chromatin fiber, which conform the chromosomes. One chromosome contains millions of base pairs. The human species contains 46 chromosomes, each of which is composed of 2,000 genes distributed throughout the DNA polymer. Fig. 2-5 shows the different phases of chromosome conformation according to the different phases of the cell cycle. The cell cycles are those phases along which a cell divides into its daughters, namely G1, S, G2, and M. The first three phases the nucleus is surrounded by a package, while mitosis is characterized by the disappearance of that package and the chromosomes appear [14].

DNA damage can be classified into direct, which are those induced directly by ionizing particle impact, and indirect, those generated by free radicals mainly produced by water radiolysis. There are a variety of damage, some as isolated lesions, known as Single Strand Breaks (SSB), which are repaired efficiently by the cell [15]. Clusters of a few SSB may lead to a damage known as Double Strand Break (DSB), which are regarded as sub-lethal lesions. It is believed that the interaction of un-repaired DSB may induce chromosome aberrations, which often are lethal.

Ionizing radiation can be classified as high LET and low LET, depending on the spatial

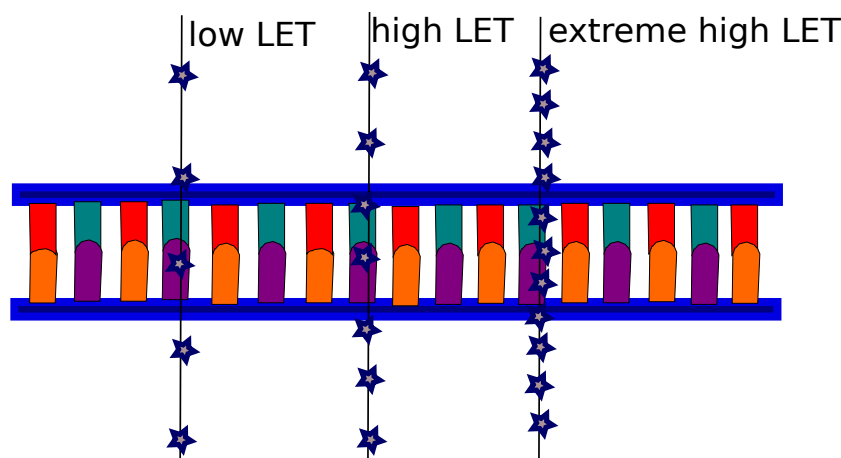


Fig. 2-5: Representation of the effect of different types of radiation on DNA: low LET, high LET and extremely high LET.

density of energy depositions and the efficiency for inducing DNA damage. While photons deposit their energy fairly homogeneously in the medium, ions deposit their energy following a very heterogeneous pattern. These energy deposits are localized close to the ion track although rare energetic delta rays can depart far from the track. This is why high LET radiation are more efficient per unit dose for inducing DNA damage.

The specific arrangement of DNA bases, namely adenine, cytosine, guanine, and thymine, constitutes the discrete genes that provide the instructions to carry out different cell processes. During the interphase, chromosomes are compartmentalized within the nucleus and have their own territories. Chromosomes are conformed by the 30 nm chromatine fibers, which are build from nucleosomes. These structures are shown in Fig. 2-6. The loops allow the packing of a large number of DNA in a small volume. Several types of proteins allow the DNA strands to be organized in a compact manner and this form of packing is usually close to that of a cylinder. Thus, cylinders can be used to emulate these structures in biophysical models, as it was done in this work.

2.9 Microdosimetry

Microdosimetry was introduced by Harald H. Rossi (1917–2000), to describe the fundamental difference between macroscopic absorbed dose distribution and energy deposition in the microscopic scale. He realized that the important quantities that describe the problem at this scale were inherently “stochastic variables” [16]. Apart from the magnitude of the dose, the spatial pattern of energy depositions for a given radiation quality has a

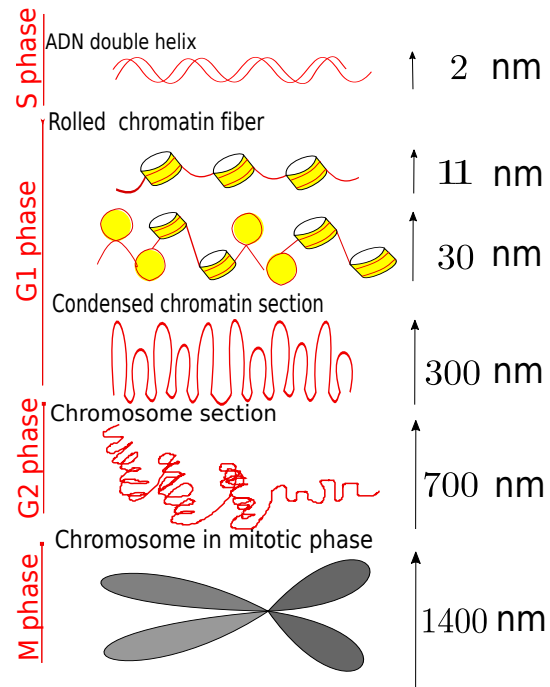


Fig. 2-6: Arrangement and scale of the bases of DNA, chromosomes, nucleosomes, and chromatin fibers.

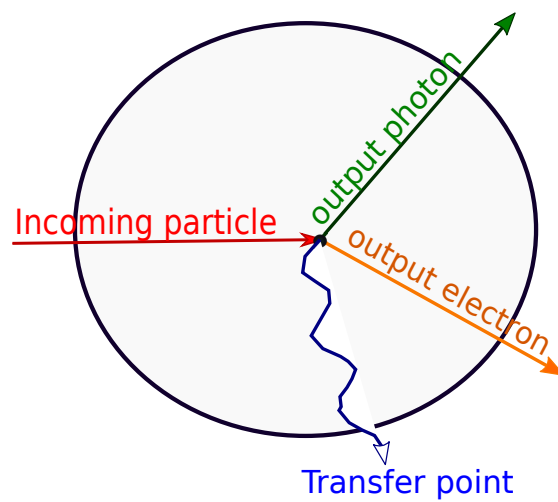


Fig. 2-7: Deposition of energy in microscopic volumes.

considerable influence on its biological effectiveness. The concept of macroscopic variables as absorbed dose and linear energy transfer (LET) already neglects the stochastic nature of ionization events. Microdosimetry aims to provide a more fundamental and general definitions.

The most fundamental quantity in microdosimetry is the deposited energy, which is the energy ϵ_i absorbed on the site of a single interaction and it is expressed by:

$$\epsilon_i = E_{in} - E_{out} + Q \quad (2-11)$$

E_{in} is the energy of incident particle, E_{out} is the energy of all particles leaving the interaction point and Q is the change in rest mass in the volume. The outgoing energy does not include of energy created inside of volume and the rest mass changes can be positive or negative. In the Fig.2-7 is represented an example of deposition of an incoming particle as photon with an incident energy, the energy deposition at a transfer point and the emission of two particles as a result of the interaction.

In one volume exist a great number of transfer point and for this reason the concept of event is used. In this case, the energy deposited in one event is $\sum_i \epsilon_i$, the sum of all energy deposits in a delimited volume, called the site. It is common to use ϵ to refer to transfer points that are caused by a single particle and its secondary particles only.

The previous definition of eqn. 2-11 is more specifically dosimetric, where ϵ is the statistical quantity whose average specific value is none other than the absorbed dose. From a microdosimetric point of view, another relation describes the spatial distribution of the elementary energy deposits in this volume; it is the imparted energy and it is expressed by

$$\epsilon = \sum_i \epsilon_i \quad (2-12)$$

The unit is always the joule (J) and ϵ can also be expressed in (eV).

If the incident particle is a charged particle, all the points where single interactions occur form the trace of the ionizing particle [17]. In fact, it is an idealization because it is assumed that the energy transferred to the environment during an elementary interaction is deposited at a particular point.

The definition of eqn. 2-12 explains the parallel between microdosimetric concepts and the principle of proportional counters. Indeed, if we admit that each point of energy

deposit represents an ionization, the proportional counter can be likened to a sphere that intercepts the trace of the particle by including none, one or more ionization's. Then, the conversion of the ionization amplitude spectra into energy deposition spectra is an important step in the experimental method that we will describe later on.

As we have seen previously, it is necessary that the volume occupied by the considered mass m is sufficiently large, because when m is too small, a value isolated of $\frac{\epsilon}{m}$ can give different information, because the absorbed doses in similar volumes can be totally different. There are therefore "minimum" volumes below in which the concept of absorbed dose can not be used.

Specific Energy

The stochastic analogous to the physical dose is the specific energy z , which is defined as:

$$z = \frac{\epsilon}{\rho \cdot V} = \frac{\epsilon}{m} \quad (2-13)$$

It is the energy ϵ absorbed in one or more than one statistically independent events in a site that has the density ρ and the volume V , the mass m .

Since the absorbed dose appears as a macroscopic concept, it is certain that the biological or chemical effects of ionizing radiation are related to the values that z can reach in certain small volumes. Thus z is the random variable defined by analogy to the absorbed dose, which is actually the average energy imparted to a volume of matter.

It can therefore be assumed that, at equal absorbed doses, the observed differences in the relative biological effectiveness of the two ionizing radiations of different nature are probably related to the fact that there are differences in the frequency with which the Specific energy z may be defined within a small volume of the irradiated material.

Lineal energy

The lineal energy y is a quantity similar to the linear energy transfer but it is defined for a given volume:

$$y = \frac{\epsilon}{\bar{l}} \quad (2-14)$$

It is defined as the energy absorbed in a single event, ϵ , along the sites mean chord length \bar{l} , which is the average length of randomly oriented chords.

The unit of lineal energy y is joule per meter ($\text{J} \cdot \text{m}^{-1}$), but $\text{keV}/\mu\text{m}$ is commonly used [18].

For convex bodies, Cauchy's theorem yields for the mean chord length $\frac{4V}{S}$, where V is the volume and S the surface of the body. For spheres, $\bar{l} = \frac{2}{3}d$, with d being the diameter of the sphere.

In conclusion, it appears that if biological phenomena are certainly correlated with the radiation linear energy transfer (LET), this magnitude is not enough to describe the energy imparted by radiation at the cellular or subcellular level. We introduce the notion of lineal energy that allows to circumvent the application limits of this variable. Indeed, lineal energy distributions describe the statistical fluctuations of the imparted energy for individual events, taking into account the variation of energy transfers, particles crossing the volume, the distribution of trajectories, the contribution of delta electrons and random electronic collisions.

Distributions and values of the weighted dose microdosimetric magnitudes.

In the previous section, it has been observed that the microdosimetric quantities are closely interrelated; thus it is sufficient to define the distribution of one of them to infer the distribution of the others.

The advantage of all these parameters lies above all in the fact that, radiobiological studies do not require any biological hypothesis, apart from the size of the volume considered [18]. Lineal energy is a stochastic quantity. It is therefore usual to consider the cumulative distribution function of y , $F(y)$, which represents the probability of obtaining the lineal energy y' less than or equal to a given value of y : $F(y) = P(y' < y)$. The probability density function $f(y)$ is defined as the derivative of $F(y)$

$$f(y) = \frac{dF(y)}{dy} \text{ and } \int_0^{\infty} f(y)dy = 1 \quad (2-15)$$

Consequently, z has the probability-density distribution $f(z)$, which is also called frequency distribution, and whose variance increases if the volume is decreased. For very small volumes, z can even be equal to zero, because the volume does not contain any transfer point. Thus, statements on z or $f(z)$ must include information about the corresponding volume V . The specific energy has the same unit as the absorbed dose [19].

The lineal energy probability density function, $f(y)$, can be used to calculate the frequency-mean lineal energy (\bar{y}_f) and the dose-mean lineal energy (\bar{y}_D) as shown in the following

equation

$$\bar{y}_F = \int_0^{\infty} y f(y) dy \quad (2-16)$$

The experimental measurement of the values of y by means of a Rossi counter leads to the frequency spectrum $N(y)$. If $N(y)dy$ represents the absolute frequency of events of magnitude y (to dy) then $\int_0^{\infty} N(y) dy$ gives the total number of events and is related to the distribution $f(y)$ by:

$$f(y)dy = \frac{N(y)dy}{\int_0^{\infty} N(y)dy} \quad (2-17)$$

All microdosimetric distributions expressed here are derived from the experimental distribution $N(y)$. The probability density $d(y)$ of the absorbed dose is also defined because it is more representative of the biological phenomenon; $d(y)dy$ is the infinitesimal fraction of the absorbed dose delivered by linear energies between y and $y+dy$. The two distributions $f(y)$ and $d(y)$ are related by the equation:

$$d(y)dy = \frac{y \cdot f(y)dy}{\int_0^{\infty} y \cdot f(y)dy} \text{ and } \int_0^{\infty} d(y)dy = 1 \quad (2-18)$$

This distribution $d(y)$ is independent of the dose rate and the absorbed dose. We express the mean lineal energy in terms of dose, non-stochastic value, as follows:

$$\bar{y}_D = \int_0^{\infty} y \cdot d(y)dy. \quad (2-19)$$

Taking into account that

$$d(y) = \frac{y}{\bar{y}_F} f(y) \quad (2-20)$$

then

$$\bar{y}_D = \frac{1}{\bar{y}_F} \int_0^{\infty} y^2 f(y)dy. \quad (2-21)$$

In the case of uniform microscopic volumes exposed to a large number of events in a uniform radiation field, the absorbed dose D is obtained through the frequency-mean specific energy \bar{z}_F for multi events

$$D \approx \bar{z}_F = \int_0^{\infty} z f(z)dz \quad (2-22)$$

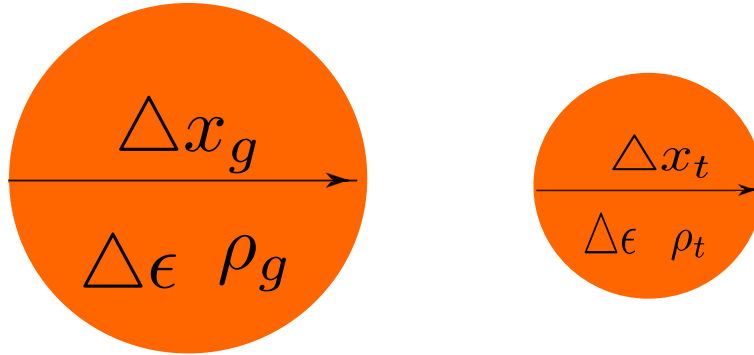


Fig. 2-8: Fano's theorem allows to replace a micrometer volume with another larger volume with a lowest density where a particle does the same deposition of energy.

2.9.1 Experimental microdosimetry

Currently, microdosimetry covers a great quantity of experimental techniques for measurement of microdosimetry variables. In the beginning of microdosimetry the device used to measure was the TCPE (Tissue Equivalent Proportional Counter), which is still used today [19]. This device was designed by Rossi and this is a sphere composed by a high pressure gas. Its performance is based to the relation of Fano [20],

$$\Delta\bar{\epsilon} = \Delta x_g \left(\frac{S}{\rho} \right)_g = \Delta x_t \left(\frac{S}{\rho} \right)_t \quad (2-23)$$

where Δx is the distance traveled by a particle, S/ρ the mass-stopping power and ρ the density, in the gas cavity or in the tissue microscopic site, it is show in the Fig. 2-8. If the detector cavity is made of "tissue equivalent" gas and walls, the mass-stopping power cancels out and its possible obtain a direct relationship of energy spectra measurement in a medium with a volume of a few millimeter with what we would be obtained in a microscopic volume. To simulate certain volume with the same deposition of energy for determinate particle should be change a density with a change of pressure. A pressure can be determinate by following formula

$$P_g = p_0 \frac{d_t \rho_t}{d_g \rho_0} \quad (2-24)$$

where terms with subscript zero correspond to normal conditions of gas

2.10 The Linear-Quadratic model

The interaction of ionizing radiation with matter is composed by a succession of low scale interactions that lead to biological effects. Despite that this process has been studied for

decades, there is still much to know about the early physico-chemical damage induced in DNA. Even more difficult is to find the connection between this initial damage and final biological effects. In general, dose-response relations are determined for biological systems, but they are not easily translated from one biological system to another, reflecting the complexity of the mechanisms involved in cells, tissues and organisms.

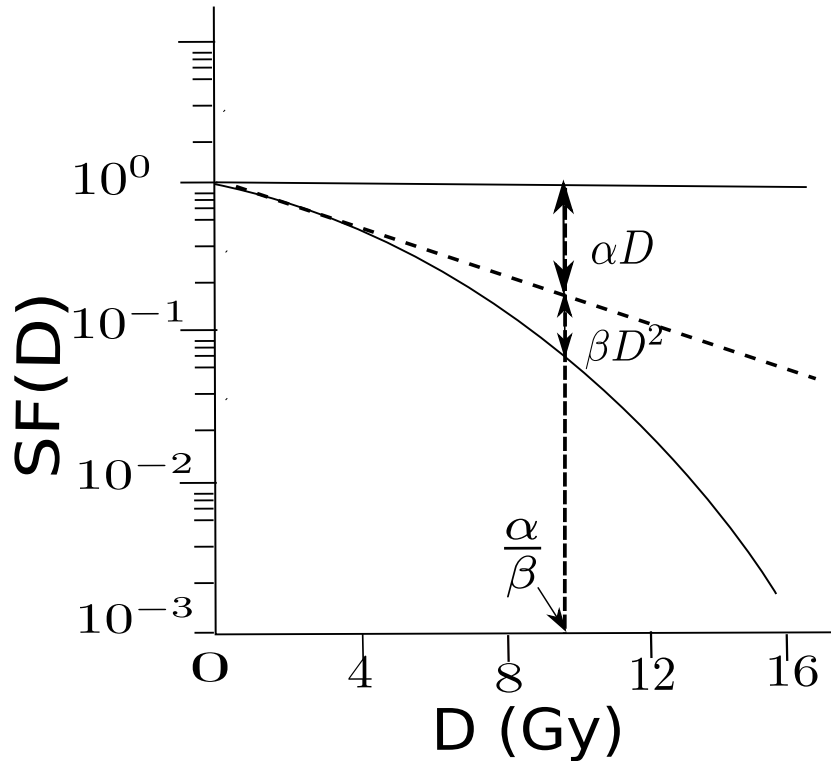


Fig. 2-9: Schematic representation of different parts of Linear-Quadratic Model

According to this relationship, what follows is that cell death can be caused either by a single lethal event (the passage of only one ionizing particle) or by the combined action of two independent sublethal lesions, related to two different ionizing particles, as Chadwick and Leenhouts have supposed in their molecular theory [21]. In fact, these lesions caused by irradiation can cause cell death depending on potential of cell in repairing their DNA. Survival curves show the ability of irradiated cells to repair themselves. The Linear-Quadratic model assumes that there are two components that are important for generating cell death due to radiation, a part that is proportional to the dose and another that is proportional to the square of the dose. The expression for the survival curve is

$$SF(D) = e^{-\alpha D + \beta D^2}, \quad (2-25)$$

where SF is the proportion of surviving cells after receiving a dose D , α is the probability of inducing a lethal damage due to one track and β is the probability same probability but when two independent tracks are involved in the same lethal damage. The the ratio α/β is the dose at which both mechanisms contribute equally to cell death.

If the survival curve has an exponential form, the rate of production of the events corresponds exactly to the rate of cellular death by lethal lesion and this type of lesions are irreparable; if the cell survival curve has a shoulder, then there is a decrease in repair capacity when the dose increases: the lesions are potentially lethal and can either evolve to an irreparable state or repair themselves. The LQ formalism describes the physical model of cell death, where the α and β factors depend on the tissue or cells in question and radiation quality.

2.11 Relative Biological Effectiveness

The Relative Biological Effectiveness (RBE) was introduced to quantify capacity of a given radiation quality to produce certain biological damage. This is defined as the ratio between the doses delivered with the reference quality and that corresponding to the quality in question, to produce the same biological effect (end point). ^{60}Co photons are commonly used as the reference quality.

Fig. 2-10 shows the survival rate as a function of dose for different radiation qualities. It can be observed that ions are more efficient to generate cell death. The RBE for a given quality X is defined as follows

$$RBE_X = \frac{D_{ref} \text{ radiation}}{D_X} \quad (2-26)$$

It should be remarked that RBE depends on the biological endpoint under considerations. It can be DSB production, chromosome aberration induction, cell death, etc. The reason for using photons as the reference quality is the large experience on their use in radiation therapy for about a century. RBE is used in hadrontherapy treatment planning as the weighting factor for obtaining the biological dose D_{bio} , which considers the biological response of tissue to a given dose and it is expressed as

$$D_{bio} = RBE \cdot D_{phys} \quad (2-27)$$

where D_{phys} is the absorbed dose. D_{bio} takes accounts the increment of biological effectiveness of ions beams when compared with photons beams. While for protons a RBE

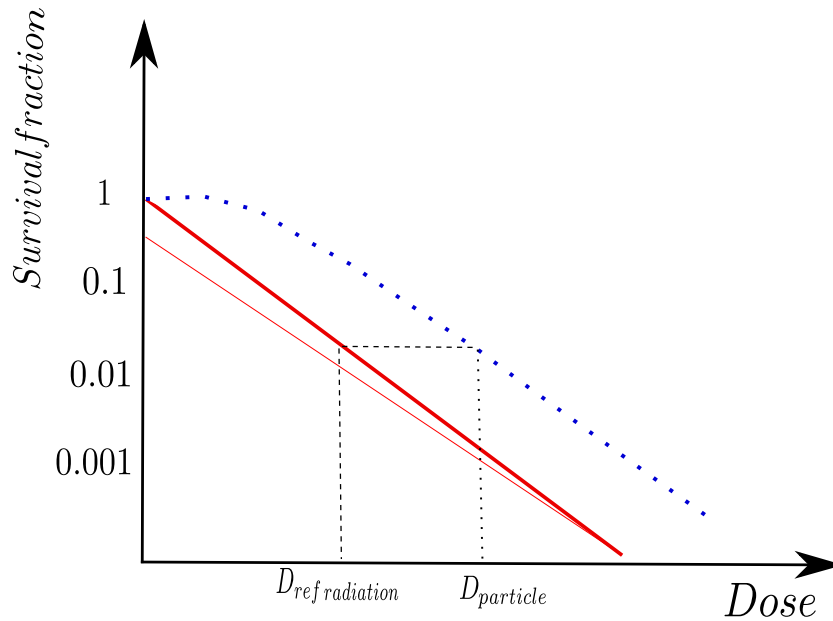


Fig. 2-10: Typical survival fraction of cell irradiated with a heavy ions (red continuous line) and other radiation of reference as photons (blue dotted line)

value equal to 1.1 has been chosen in the case of energetic ions, the case of energetic heavier ions is more complex since it depends strongly with the energy, which depends on the penetration depth. The main physical features of heavy charged particles relevant for the RBE the charge and speed of the particle. Biological aspects include tissue type, oxygen concentration, among others.

2.12 RBE models

Particle therapy delivered either with protons, carbon, or other ions has unique biological effects when compared to photon therapy. To optimize the clinical outcome of particle therapy, it is necessary to estimate the relative biological effectiveness (RBE) of particle beams. RBE represents a key information during the treatment planning process in hadrontherapy. The RBE is defined as the ratio between the dose needed to produce a given effect with a reference radiation quality to that necessary to induce the same effect with the radiation in question.

Currently, protons are believed to have RBE slightly higher than photons while carbon ions have RBE several times that of photons. Many factors influence RBE such as the absorbed dose, the radiobiological characteristics of the cell, tissue, or tumour, and the

local ionization density or clustering which is related, at first approximation, to the linear energy transfer (LET). The LET is determined by the quality of the radiation, mainly by the charge to speed ratio. This multitude of factors introduces large uncertainties into the RBE values to be used for clinical treatment planning. As said just above, RBE depends strongly on the biosystem in question. In general, radiosensitive biosystems have high α/β ratios and small RBE values, and radioresistant systems have small α/β ratios and high RBE values.

In Japan, considerable progress was made in developing RBE predictive models based on fast neutron RBE data which allow good estimation of RBE for carbon ions. More recently, the microdosimetric kinetic model (MKM) based on original insights by Hawkind in the United States has been used in Japan. This model assumes that the RBE is determined by the specific energy distribution in domains with size similar to that of the cell nucleus.

In contrast, the German carbon-ion beam projects at GSI have gathered experience in the use of the local effect model (LEM). It incorporates a microdosimetric theory which is extrapolated to cell survival curves. The dose profile was controlled by the LET profile and there has been far less variation in dose per fraction compared with the MKM.

Such refinements have not been used for proton beams where a fixed RBE of 1.1 is assumed, so a uniform physical dose rather than a biologically equivalent dose profile is delivered. It remains to be seen if more detailed LET mapping with appropriated dose weighting based on predictive RBE models will be used. At the very least, before such a sophisticated approach is developed and employed, it may be expedient to assume simpler generic changes in RBE depending of tissue.

2.12.1 RBE Measurements

In many studies, the RBE for carbon ions clearly correlates with photon radiosensitivity, exemplified by cell lines deficient in DNA repair pathways, which are more sensitive to photons. Conversely, many tumors are characterized by genetic alterations, which confer radioresistance. Some mutations are able to cause a restricted response to cellular stress, often associated with increased resistance to low-LET ionizing radiation. Similarly, in cancerous cells, proteins involved in the suppression of apoptosis make cells resistant to radiation. Compared to conventional radiation, cell inactivation after exposure to high-LET particles is more pronounced in such systems, which results in a higher RBE.

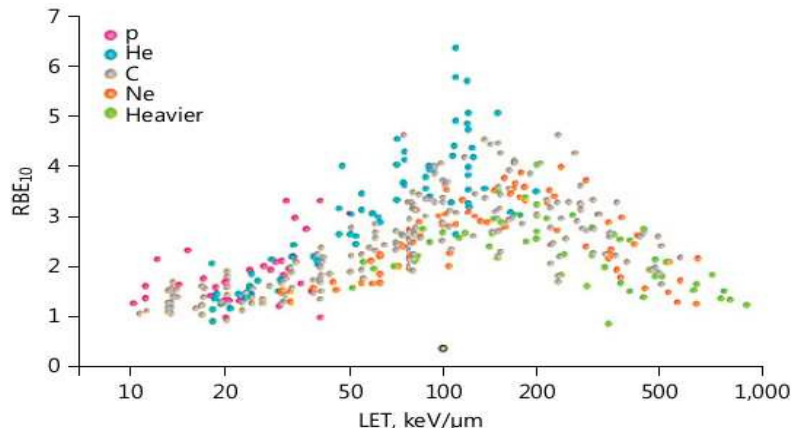


Fig. 2-11: RBE as a function of the LET. The example depicts a 10% clonogenic cell survival as the biological endpoint

Recent findings indicate the existence of glioblastoma cells with radioresistance to both low- and high-LET radiations, presumably associated with the status of their intrinsic genome integrity. Likewise, some sub-clones of cancer cells become radiation resistance by repeated exposure to X-rays and also reveal resistance to carbon ions, pointing to a damage-response independent of the radiation quality.

Friedrich et al. [23] established a large particle irradiation data ensemble based on published cell survival curves after irradiation with different ions and analyzed the RBE as a function of LET and α/β ratio, the frequency distributions of α and β parameters among different cell lines. Fig. (2-11) shows the RBE₁₀ as a function of the LET for several ions [22,23]. This RBE uses the 10 % survival fraction as biological endpoint. Fig. (2-12) depicts the RBE _{α} as a function of LET, which is also known as the maximum RBE or zero-dose RBE.

2.12.2 Animal models

In clinical situation, there is still a lack of knowledge about the response of various tumor types, as well as of early and late responding normal tissues. While cell lines are predominantly useful to search for underlying mechanisms, whole animal models are helpful to validate tolerance doses, fractionation effects, and clinical efficiency.

Determining normal tissue RBEs is of outstanding relevance because (i) correlation of

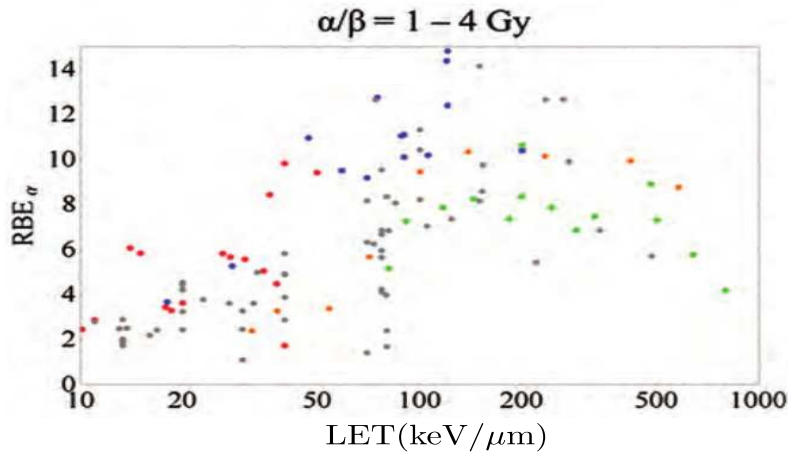


Fig. 2-12: RBE as a function of the LET with shouldered $\alpha/\beta = 1-4 \text{ Gy}$. In this figure the nomenclature is p: red; He: blue; C: gray; Ne: orange; ions heavier than Ne: green

LET and RBE is not necessarily linear across a complete range and may also depend on the dose per fraction, (ii) in spite of the high physical accuracy, a non-negligible volume of normal tissue surrounding the tumor is in close proximity to the planning target volume (PTV) (iii) all solid tumors contain normal tissue structures, such as stromal structures and vascular elements, and many tumor cells are intertwined in a normal tissue.

Radiation-induced normal tissue lesions reveal differences in their temporal appearance. Early effects occurring with the onset of radiation are associated with cell inactivation of rapidly proliferating radiosensitive cells, increased endothelial cell swelling, vascular permeability, and edema as well as lymphocyte adhesion and infiltration. Recovery processes start with repair and repopulation of stem cell pools within individual tissue compartments and, depending on the turnover time of the tissue, continue for months [24].

2.12.3 Clinical models

Due to the complex dependence of the RBE on physical and biological factors, RBE values always refer to the specific irradiation conditions, the biological system as well as to the selected biological endpoint. The resulting RBE is therefore more accurately termed as ‘experimental RBE’. With this respect, all RBE values are experimental and when referencing these values, the experimental conditions have to be clearly specified. In contrast, the ‘clinical’ RBE describes the ratio of the prescribed absorbed dose for the reference quality, usually photons, and that for the high-LET radiation, which is believed

to result in clinically equivalent results. In contrast to the experimental RBE, the clinical RBE is an operational concept, which involves a medical decision on the basis of all currently available experimental and clinical information and with increasing experience, the clinical RBE may be adjusted.

RBE based on survival curves

In terms of the parameters of the linear-quadratic model (LQM) [25], this shows an increased intrinsic radiosensitivity and a reduced repair capacity, which both are LET-dependent. As a direct consequence of the different shapes of the survival curves, the RBE becomes dependent on dose. And through the parameters obtained in the fitting of survival curves, we can calculate of RBE with the following relation:

$$RBE = \frac{-(\frac{\alpha}{\beta})_{ph} + \sqrt{(\frac{\alpha}{\beta})_{ph}^2 + 4(\frac{\alpha}{\beta})_{ph}RBE_{max}d_{ion}[1 + \frac{d_{ion}}{(\alpha/\beta)_{ion}}]}}{2d_{ion}} \quad (2-28)$$

where $RBE_{max} = \alpha_{ion}/\alpha_{ph}$ is the maximum RBE given by the initial slopes of the survival curves and $(\alpha/\beta)_{ph}$ and $(\alpha/\beta)_{ion}$ are the repair capacities for photons and ions, respectively.

Mixed beam model

For carbon ion therapy with passive delivery techniques, a phenomenological model was developed at the National Institute of Radiological Sciences (NIRS) [26]. In this model, the RBE is calculated from the cell survival curves for photons and ions using a specified survival level. The basic idea of the model is to determine the LET dependence of the curve parameters α and β for monoenergetic ion beams *in vitro* and to transform these values into effective values $\alpha_{mix}(x)$ and $\beta_{mix}(x)$ for a LET spectrum ('mixed beams') located at the depth x within an SOBP by

$$\alpha_{mix}(x) = \sum_i \frac{d_i(x)}{D(x)} \alpha_i \quad (2-29)$$

and

$$\sqrt{\beta_{mix}(x)} = \sum_i \frac{d_i(x)}{D(x)} \sqrt{\beta_i} \quad (2-30)$$

In the previous equations, $d_i(x)$ is the dose contribution of beam i at the depth x and $D(x)$ is the respective total dose of all contributions to the SOBP. The values of the curve

parameters α_i and β_i for beam i at the depth x reflect the LET dependence of the survival curve. The RBE relation for this model is shown below:

$$RBE = \frac{2\beta_{mix}(x) \cdot D_{ph}(S)}{-\alpha_{mix}(x) + \sqrt{\alpha_{mix}^2(x) - 4\beta_{mix}(x) \cdot \ln(S)}} \quad (2-31)$$

The LEM formalism

To predict cell survival, the Local Effect Model (LEM), considers that cell killing arises from the induction of lethal lesions by the ionizing radiation. Assuming that the distribution of lethal lesions obeys a Poisson distribution, the probability for the cell to survive reads:

$$S(D) = e^{-N_{lethal}(D)} \quad (2-32)$$

where $N_{lethal}(D)$ is the mean number of lethal lesions induced in the cell after a dose D . The first key assumption of the LEM is to consider lethal lesions as point-like events generated by the local dose deposited by the radiation. Thus, the number of lethal lesions in the cell is the summation of the local lethal lesions over the cell sensitive volume:

$$N_{lethal}(D) = \iiint_{Sensitive\ Volume} \rho_{lethal}(\mathbf{r}) d\mathbf{r} \quad (2-33)$$

In the LEM, the local dose is calculated by cumulative effects, superimposing the local dose deposited by each ion, which is represented by the radial dose d_R :

$$d(r) = \sum_i d_R(r_i), \quad (2-34)$$

Where r_i is the radial distance of the point \mathbf{r} to the trajectory of the i^{th} ion in the cross plane to the beam axis. The second key assumption of the LEM consists in extracting the relation between the density of lethal lesions and the local dose from survival measurements performed with X-ray radiation. Indeed, the local dose deposited by X-ray radiation is considered as uniform within the cell. Neglecting stochastic effects, it is therefore equal to the macroscopic dose D . $N_{lethal}(D)$, and therefore $\rho_{lethal}(D)$ can be deduced from the measurement of cell survival to X-ray irradiation (described by the α and β parameters) and from an estimation of the cell sensitive volume V . This latter is assumed to be uniformly distributed over the cell nucleus. The diameter of the sensitive volume depends on the cell and ranges from 5-20 μm . An explicit expression for the average number of lethal lesions can thus be obtained as:

$$N_{lethal} = \iiint_{Sensitive\ Volume} \frac{-\ln S_X(d(r))}{V_{sensitive}} dV \quad (2-35)$$

The MKM formalism

The MK model is based on the statistical theory and microdosimetric quantities. In this model, lesions are produced in sub-volumes of the cell nucleus called "domains". The dose deposited in these domains is quantified by the so-called "specific energy" z , which is a stochastic quantity. Lesions are classified into two different types, Type I are lethal and non-repairable, type II are initially not lethal but may become lethal if they undergo some specific transformations. The probability of forming a type I lesion in a domain is proportional to the specific energy imparted to that domain. Non-lethal type II lesions may be repaired or transformed into lethal lesions.

For a short time irradiation and assuming a Poisson distribution of lethal lesions, the mean number of lesions in the nucleus is expressed by:

$$\epsilon(D) = \alpha_p D + \beta D^2 \quad (2-36)$$

Where the index p indicates the Poisson distribution; $\alpha_p = \alpha_0 + \beta \bar{z}_{1D}$ and α_0 and β are cell-dependent but LET independent parameters; \bar{z}_{1D} is the single event dose-mean specific energy in the domain. Therefore the expression of RBE in the limit of zero dose is given by:

$$RBE = \frac{\alpha_0}{\alpha_R} + \frac{\beta}{\alpha_R} \bar{z}_{1D} \quad (2-37)$$

Replacing \bar{z}_{1D} by its expression versus the mean dose lineal energy y_D assuming spherical domain, equation reads:

$$RBE = \frac{\alpha_0}{\alpha_R} + \frac{\beta}{\alpha_R} \frac{0.2}{d^2} \bar{y}_D \quad (2-38)$$

This expression allows deducing the two parameters α_0 and the domain diameter d by fitting experimental data for LET below the saturation effect. The value of β is deduced from the X rays radiation and assumed to be unchanged with changing LET or particle type [27].

3 The Monte Carlo methods in microdosimetry

The first reference that has a numerical simulation of a random event was around the year 1733, in which the experiment of the Buffon's needle is described. This consisted in throwing the needle on a sheet with parallel stripes a number of times, between which there was a distance $a \leq l$. From this experiment, the probability that the needle crosses any of the lines is $p = \frac{2a}{\pi l}$ [28]. From this problem, in a way to determine the value of π . Subsequently, with the development of computers and the need to make numerical numbers of random events the methods known as Monte Carlo arose. The Monte Carlo methods were developed in 1949 in los Alamos Laboratory by Neumann who was a leader of Theoretical Division, it was developed as a statistical approach to solving neutron diffusion and multiplication problems.

Monte Carlo method is a non-deterministic or numerical statistical method, used to approximate complex mathematical expressions. So, with the Monte Carlo method what is done is a kind of nature mimicry, giving rules for objects interaction and repeating the process in a random way. In principle, it is a technique that allows us to obtain an approximation of a macroscopic system from the simulation of its microscopic interaction. This method is used as statistical approximation for integro-differential equation solutions. Before applying Monte Carlo methods it is necessary to have a description of physics problems in terms a mathematical equation or system of equations. This means that Monte Carlo methods are not only implicated to problems involved in random events. Samples are generated and a solution for statistical problems is founded with estimation of distribution parameters. The end value has a statistical uncertainty, in addition to any systematic error.

Monte Carlo methods are used a wide range of problems. Civil engineers are applying it for traffic planning, electrical engineers apply it to simulate electronic transport in semi-conductor devices, and investors use it to forecast risk . In bioinformatics, Monte Carlo's techniques are applied for genetic modeling. In mathematics, it is used to solve

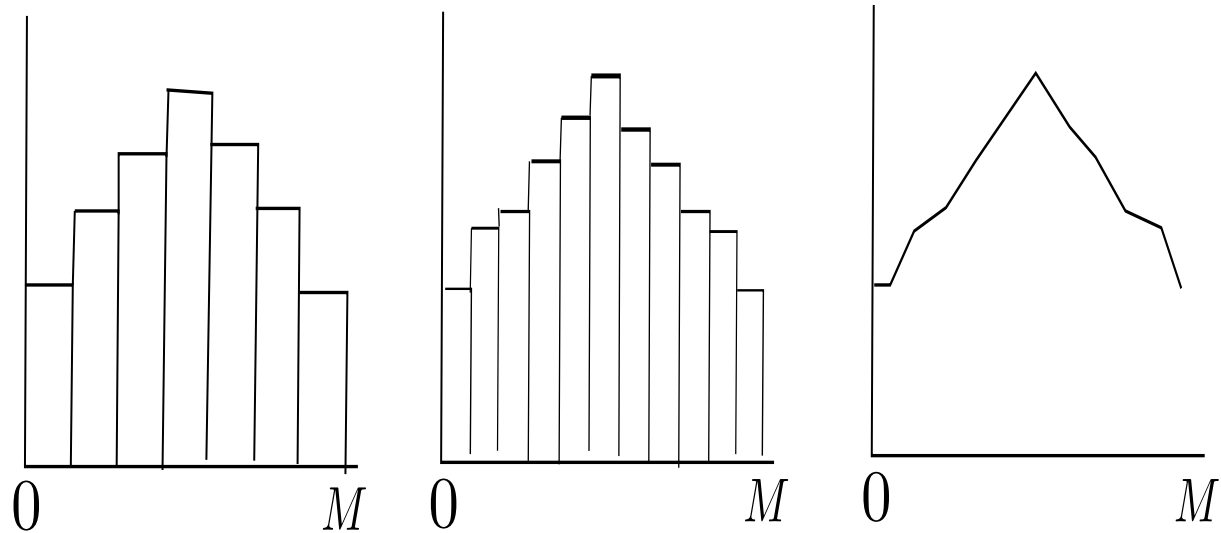


Fig. 3-1: Measurement histogram to the nearest meter, to the nearest centimeter and the limit to a continuous function

complicated integrals.

3.1 Fundamentals of the method

3.1.1 Probability theory

A discrete random variable is one whose possible values constitute a finite set or an infinite sequence of elements. A random variable whose set of possible values is a complete range of numbers is not discrete. A random variable X is continuous if a) its possible values comprise a single interval on the numbering line $A < x < B$ or a union of disjoint intervals. b) $P(X = C) = 0$ for any number C that is a possible value of X .

An example of this is the study of the ecology of a lake, the depth is measured in selected places, then, $X =$ the depth in that place, this is a continuous variable. In this case, A is the minimum depth in the sampled region and B is the maximum depth. Now suppose that X is discretized by measuring the depth to the nearest meter, so that the possible values are nonnegative integers less than or equal to B . The resulting discrete distribution is illustrated with a probability histogram as shown in the Fig. 3-1. If you draw a histogram so that the area of the rectangle over any integer is k . On the other hand, if the depth is measured more accurately and the same measurement axis is used, each resulting probability is narrower, even if in the total area of all the rectangles it remains

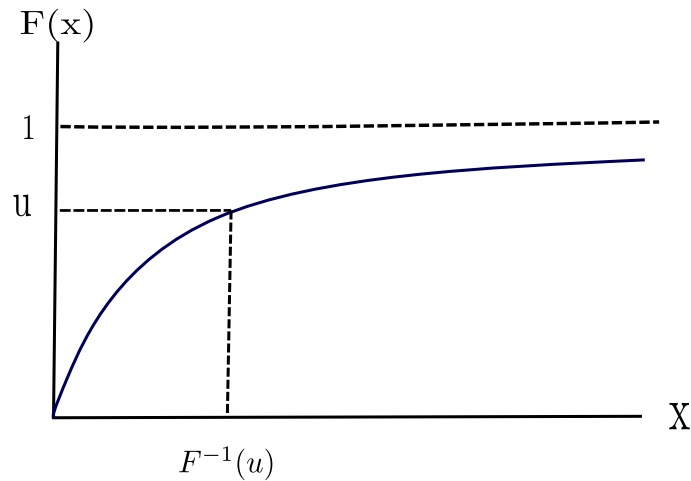


Fig. 3-2: Inverse method

1 [29].

Given the random variable X with a distribution of the cumulative probability function $F(x) = P(X \leq x)$, the function $F(x)$ must be a growing function in x and its inverse function F^{-1} , must be defined for any value of z between 0 and 1, such that the smallest x satisfies $f(x) \geq z$. The above can be written through the mathematical definition

$$F^{-1}(z) = \inf \{x | F(x) \geq z\} \quad (3-1)$$

for $0 \leq z \leq 1$, where $F^{-1}(0) = -\infty$

if the random number U is obtained by a uniform distribution in the interval $[0, 1)$, then the continuous variable X is given by:

$$X = F^{-1}(U) \quad (3-2)$$

3.1.2 Sampling theory

Invertible cumulative distribution function

Formally, let X be a random variable, then, a probability or probability density distribution $f(x)$ such that for any two numbers a and b , with $a \leq b$

$$P(a \leq X \leq b) = \int_a^b f(x) dx \quad (3-3)$$

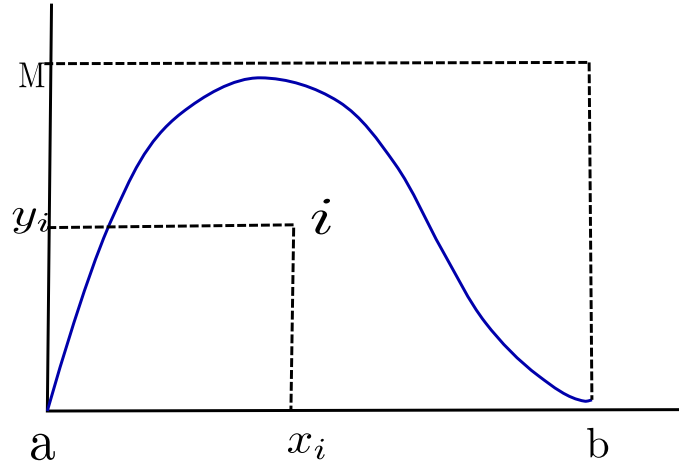


Fig. 3-3: Rejection and acceptance method

that is the probability that X assumes a value in the interval $[a, b]$, also it is the area over this interval and under the graph of the density function.

The cumulative distribution function $F(x)$ of a discrete random variable X gives, with any specified number x , the probability $P(X \leq x)$. It is obtained by adding the probability mass function $p(y)$ along all possible values and satisfying $y \leq x$. The cumulative distribution function of a continuous random variable with a given probability function, $P(X \leq x)$, is obtained by integrating the probability density function $f(y)$ between the limits $-\infty$ and ∞ . The cumulative distribution function of a random variable X is defined by every x number as

$$F(x) = P(X \leq x) = \int_{-\infty}^x f(y)dy \quad (3-4)$$

With each x , $F(x)$, the area is under the density curve to the left of x .

The probability functions can be characterized in terms of their moments

$$\langle x^n \rangle = \int_{x_{min}}^{x_{max}} x^n p(x) dx \quad (3-5)$$

When it can be guaranteed that the existence of the moments $\langle x \rangle$ and $\langle x^2 \rangle$ exists, the variance can be calculated with the following expression

$$var(x) = \langle x^2 \rangle - \langle x \rangle^2 \quad (3-6)$$

Rejection and acceptance method

The acceptance and rejection method simulates a value of the random variable X with probability density function $f(x)$ bounded in the interval (a, b) . Let M be a value such that $M \geq f(x)$ for all $x \in (a, b)$. The procedure consists in generating points randomly in the base rectangle (a, b) and height $(0, M)$. The coordinates of the point i are given by the pair (x_i, y_i) , as shown in the Fig. **3-3**. If the point falls within the graph of the density function, its coordinate x is accepted as the random variable value with density function $f(x)$; otherwise the point is rejected and another must be generate. Accepted points are evenly distributed under the curve $f(x)$ [30].

Since the probability that a point falls under the curve is equal to the quotient between the number of points accepted and generated, the distribution of accepted values has a $f(x)$ as a function of probability density [31]. The method consists in generating a value of the random variable and testing whether said value comes from the probability distribution that is being studied. So, if generating a random number R it must be fulfilled that

$$R < \frac{f(x_i)}{M} \quad (3-7)$$

3.1.3 Random number generator

The core of the simulations of random models is the ability to generate random numbers, which represent the value of a random variable with uniform distribution. A random number generator is a specific formula that produces random numbers in a completely deterministic way. For this reason, random numbers generated either by manual or computational methods, are called pseudo-random numbers. One of the most common method for generating random numbers starts by setting positive integers m , a and $norm$. The process is initialized with a number called seed, which satisfies that

$$0 \leq seed \leq norm, \quad (3-8)$$

then, the other numbers are generated from this initial value using the formula

$$seed = (m \cdot seed + a) \text{mod } norm \quad (3-9)$$

The numbers $seed$, m , a and $norm$ must satisfy certain conditions. First, the seed must be greater than 1 and it must not exceed the whole maximum that can be stored by the computer and it must be a random number. The idea that this seed is random has the purpose of assuring that each sequencing of numbers is different. One way to choose a seed is by means of the "clock" command that gives a vector of 6 components corresponding to the year, month, day, minute and second [32].

3.1.4 Monte Carlo Method in radiation transport

Monte Carlo's method has been used in the study of random phenomena as radiation transport. Simulations require a total, partial and differential cross sections. The process to follow is outlined below. For every interaction there is a probability density to some distance z , which is given by

$$p_s(z) = \mu e^{-\mu z} \quad (3-10)$$

The above expression is known as the law for the probability of survival of the particles as a function of depth. The cumulative probability is

$$P_s(z) = \int_{-\infty}^z p_s(z) dz = 1 - e^{-\mu z} \quad (3-11)$$

The particles interact with atoms and molecules to be targeted by several mechanisms: elastic and inelastic collision, photoelectric and coulomb effects, etc. Every interaction is characterized by a cross section σ and the number density of the target particles, n . The mean free path λ is defined as the average path length between collisions and it is described by following relation

$$\lambda = \int_0^{\infty} z p_s(z) dz = \frac{1}{\mu} = \frac{1}{n\sigma} \quad (3-12)$$

Taking into account a particle moving with an energy E , in every interaction a particle losses certain amount of energy W and changes its direction. The angular deflection is determined by a polar angle which correspond to the angle between direction to particles before and after scattering, and the azimuthal angle ϕ . These variables are generated randomly. Every particles trajectory starts in a given position and energy in agreement with source characteristics. The particle state immediately after of interaction is defined by position coordinate $\bar{r} = (x, y, z)$, an energy E and director cosines $d = (u, v, w)$. The trajectories generation begins with a superposition of particles with a state r , E and d . Lengths s of mean free path to the following collision are generated with a samples formula

$$s = -\frac{1}{\mu(E)} \log(1 - r) \quad (3-13)$$

where r is uniformly distributed and it takes values between 0 and 1. Provided this value s , the step for transport can be executed by means of $x = x_0 + us$ [30].

3.1.5 Monte Carlo Uncertainties

There are two approaches for estimating uncertainties in Monte Carlo simulations. These are batches and variance methods,

Variance method

It is a direct method in which a variable x is calculated during the course of the Monte Carlo simulation and his value is scored. The average value calculation of the of said variable is

$$\bar{x} = \frac{1}{N} \sum_{i=1}^N x_i \quad (3-14)$$

The variance associated with the distribution of x_i

$$s_x = \frac{1}{N-1} \sum_{j=1}^n (x_j - \bar{x})^2 \quad (3-15)$$

The estimated variance of x is the standard variance of the mean:

$$s_{\bar{x}}^2 = \frac{s_x^2}{N} \quad (3-16)$$

To report the final result we must do

$$x = \bar{x} \pm s_{\bar{x}} \quad (3-17)$$

Batches method

In the Batch methods the simulations are divide the simulations of N histories into n equal batches and calculated in the standard error on the mean S_x for the simulated quantity x

$$s_x = \sqrt{\frac{\sum (x_i - \bar{x})^2}{n(n-1)}} \quad (3-18)$$

where \bar{x} is the mean value of x

$$\bar{x} = \frac{1}{n} \sum_{j=1}^n x_j \quad (3-19)$$

The estimated variance of x is the standard variance of the mean:

$$s_{\bar{x}}^2 = \frac{s_x^2}{n} \quad (3-20)$$

The result can be reporting as $x = \bar{x} \pm s_x$.

3.2 Monte Carlo Codes

Simulations with Monte Carlo method were applied quickly to the area of medical physics in 1960, with the purpose of calculating the deposited doses of the radiation in macroscopic volumes. All these codes are developed for applications that require the transport of particles such as electrons, photons and ions. In addition, these codes use the condensed history technique, where calculation times are optimized. Many of them are the basis of many programs of commercial use in clinics. The main codes used will be shown below, in which the type of particles, target materials and energy ranges will be indicated.

3.2.1 EGS

EGS(Electron Gamma Shower) [33] is a code developed by SLAC National Accelerator Laboratory originally designed for high energy applications which allows to simulate different geometries for electrons and photons. With an extension in the low-energy, it begins to be used in medical physics. A version of this code was developed, known as EGSnrc, this was developed with the purpose of doing dosimetry simulations . In this code, there are available calculations about dose distributions, particle fluency and stopping power ratios.

3.2.2 FLUKA

Fluka is a general purpose particle and heavy ion transport and interaction code which is developed and maintained in the framework of an agreement between the European Laboratory for Particle Physics (CERN) and the Italian National Institute for Nuclear Physics (INFN). It is capable of handling the transport and interactions of hadrons, heavy ions and electromagnetic particles from a few keV (or from thermal energies for neutrons) up to cosmic ray energies in whichever solid, gas or liquid material. Fluka is used for a vast variety of applications like proton and electron accelerator shielding applications, target design, calorimetry, activation, dosimetry, detector design, Accelerator Driven Systems, space radiation and cosmic ray showers, neutrino physics and radiotherapy. Particles can be transported in arbitrary complex geometries, which can also include magnetic fields. For therapeutic application a module which handles voxel geometries like CT scans, is available. Fluka is constantly updated and extended. A description of recent developments can also be found [34].

3.2.3 MCNP

MCNP is a general Monte Carlo N-Particle transport code. It can be used to model photons with energies from 1 keV to 100 GeV and other types of particles including neutrons, electrons, light ions, and heavy ions over a wide range of energies. Although, MCNP can define arbitrary geometry configurations for simulation of radiation transport. In MCNP the particle can be configured as a source and the user can define the physical rules and the result of every interaction is supported by a random number generation. Ultimately, MCNP allows the user to simulate radiation transport and tally the results of the simulation by using input that defines the geometry, particle characteristics, materials, and type of tally desired. Great care is required in defining a MCNP simulation because the simulation is only as accurate as the input definition of the simulation.

3.2.4 PENELOPE

PENELOPE is an acronym of Penetration and Energy Loss of Positrons and Electrons, it is an open software coded in FORTRAN 77. With this Monte Carlo simulation package it is possible to describe the transport of electrons, photons and positrons in any material and a range of energy from 50 eV to 1 GeV. PENELOPE allows us to use elaborate simulation for photon transport, a mixed scheme for electrons and positrons. Mixed simulation is consistently employed for all interaction mechanisms; that is, elastic, inelastic, and radiative collisions. It is feasible to introduce certain defined parameters to use it for a controlled particles transport. These parameters are cutoff energies for hard inelastic and hard bremsstrahlung events, the maximum allowed step length, limit the average angular deflection and the maximum average energy loss between consecutive hard elastic events.

3.2.5 ETRAN

The ETRAN system uses the Class of condensed history algorithm. It was originally developed for low-energy electron transport, up to a few MeV. The code was later extended to include coupled photon-electron transport for energies up to 1 GeV. ETRAN has been benchmarked extensively, but it is not user-friendly.

3.2.6 Geant4

GEANT is a project started in 1993 with a version of geant3, which was developed in FORTRAN. Later, in the year 1998, a geant version was implemented entirely in C++ and

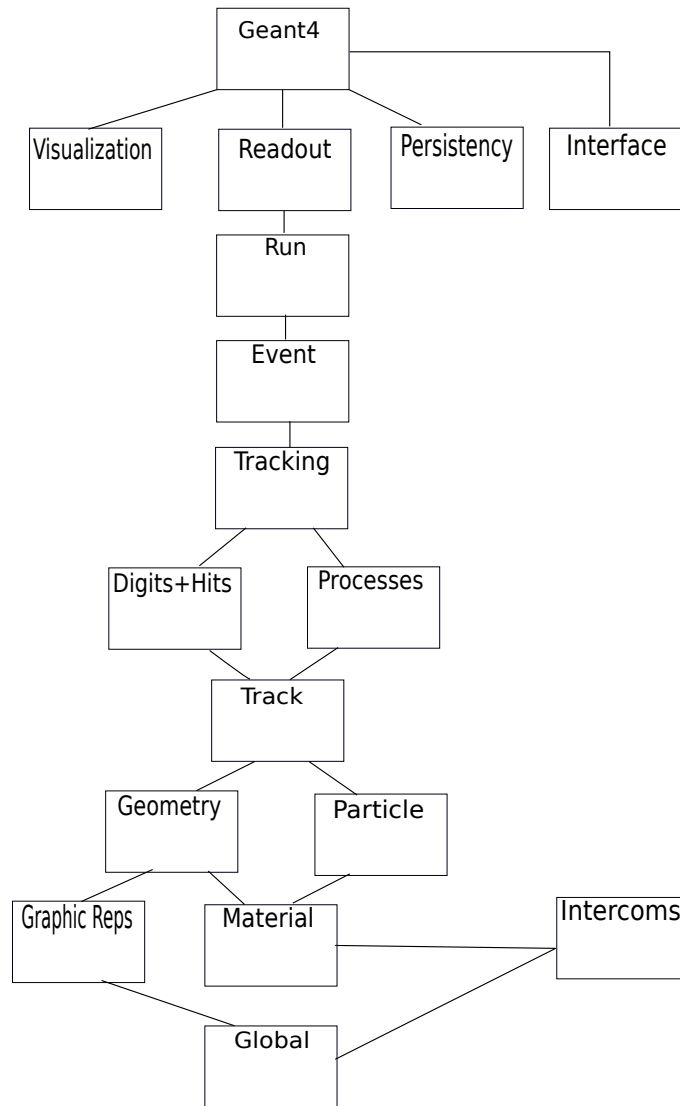


Fig. 3-4: Structure of geant4

known as geant4. Both particle codes were performance for modeling complex geometries for applications simulations involving transport of radiation in a matter. GEANT4, using the object-oriented programming, allows the code to have greater flexibility and expansibility compared with the other FORTRAN-based Monte Carlo codes. While the development of its predecessor GEANT3 has been stopped, since 1994, GEANT4 is being upgraded by a collaborating institutes.

Geant4 is a toolkit composed by a broad and different library classes that allows the users to build their own program. Some of them are mandatory and another are used for the user to access to process information. In the Fig. **3-4** the structure of geant4 is shown [35].

Mandatory classes

In any application there must be at least three classes. These will be G4VUserDetector-Construction, G4VUserPhysicsList, and G4VUserPrimaryGeneratorAction. This classes are controled by a run manager. All of them are important to define basic aspects of the program stories such as the detector definition, a definition primary particles sources and a definition of physics lists.

In the detector definition the geometry of system is configured . For this, a world volume must be defined. This volume will be the largest and here, we will define the geometry of the system with daughter volumes. There are several steps to build the system geometry which will be summarized below

1. Geometric Volume = Construction of a solid matter with specific form and dimensions.
2. Logical Volume = Geometric Volume + Material. It is built from the G4LogicalVo-class volume
3. Logical Volume= Location in the reference system that can be a logical volume or the world. It is built starting from class G4VPhysicalVolume.

We had mentioned before that the other mandatory classes are a primary generator. It must be implemented using the class G4UserPrimaryGeneratorAction. This is responsible for generating the primary particles within the simulation, as well as its functions of energy distribution, position and momentum. A wide variety of physics processes can be simulated using GEANT4. These processes are grouped into seven categories: electromagnetic, hadronic, decay, optical, photolepton hadron, parameterization, and transportation.

For radiotherapy applications, the transportation and electromagnetic processes are required. When we invoke to method initialize() de G4RunManager, Geant4 verifies the existence of these three classes.

Action classes

Geant4 provides five classes of action for the user that allows us to extract and analyze the information obtained in the different stages of the simulation. These classes are in particular: G4UserRunAction, G4UserEventAction, G4UserStrackingAction.

3.2.7 Geant4-DNA project

The geant4 DNA project started at the head of the Niemine DR of the European space agency with the purpose of developing useful simulations for the description of ionizing radiation in a radiological protection context for the preparation of future space expeditions that would allow the human being to inhabit long temporal periods in space. Currently, this project is a free platform for the use of the scientific community that carries out innovation in the modeling of the ionizing radiation interactions with the biological medium and the water molecule.

This project has three fundamental axes of development: physical stage, physico-chemical stage and biological stage. The physical stage that seeks the development of processes that model step by step the particles interactions with the biological medium, which is considered mainly constituted by liquid water and in some other cases already more specifically with the nucleobases materials. The chemical physical stage consists in modeling the production, diffusion, and interactions of molecular species and free radicals created by the radiolysis of water [36].

3.3 Geant4 physics models for microdosimetry and nanodosimetry

3.3.1 Inelastic models for electrons

The electrons inelastic processes play a fundamental role in the simulation of ionizing radiation effects, since these are the origin of elementary depositions in the biological material. When an electron crosses a water volume it loses its energy in the interaction with the medium electrons through of three main processes

- Elastic scattering, which dominates at energies lower than 1 keV.

Transition	Geant4-DNA Threshold Energy (eV)
A^1B_1	8.10
B^1A_1	10.10
Rydberg A+B	12.00
Rydberg C+D	13.51
Diffuse Band	14.41

Tab. 3-5: Excitation energies of liquid water used in Geant4-DNA, obtained by empirical fit of optical data

- Electronic excitation that takes into account 5 states: A^1B_1 , B^1A_1 , Ryd $C + D$ and the diffuse bands (see Tab. 3-5).
- Ionization of the 4 valence layers of the molecule: $1b_1$, $3a_1$, $1b_2$, and a_1 , besides the K-shell of oxygen.

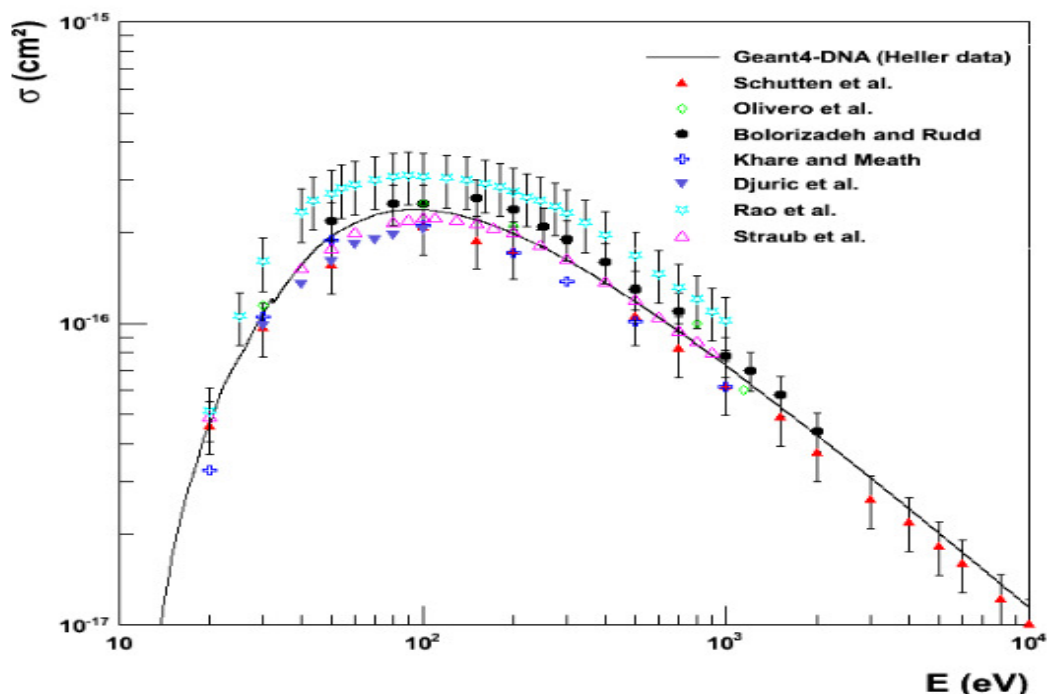


Fig. 3-6: Total ionization cross sections for electrons obtained by different models.

For the determination of the cross sections for electrons and other charged particles at high speeds, it is most efficient to use the framework of the Bethe theory, based on the first Born approximation (FBA). The Born theory can be applied both for electronic excitation and valence shell ionization.

$$\frac{d^2\Sigma}{dEdK} = \frac{1}{\pi a_0 T} \frac{\eta_2(E, K)}{K} \quad (3-21)$$

where Σ is the macroscopic cross section, E and K are the energy and momentum transfer, respectively. The macroscopic cross section can be obtained as

$$\Sigma = N\sigma, \quad (3-22)$$

where $N = \rho \frac{N_A}{A}$ is the number of molecules per volume unit, ρ is the density of the material, N_A is the Avogadro number, a_0 is the Bohr radius, and T is the kinetic energy of the incident electron. $\eta_2(E, K)$ is the electronic loss function, which represents the Bethe surface.

The single differential cross section is obtained by integrating the double differential cross section between K_{min} and K_{max}

$$\frac{d\Sigma}{dE} = \frac{1}{\pi a_0 T} \int_{K_{min}}^{K_{max}} \eta_2(E, K) \frac{dK}{K} \quad (3-23)$$

where

$$K_{min} = \frac{\sqrt{2m}}{\hbar} (\sqrt{T} - \sqrt{T - E}) \quad (3-24)$$

and

$$K_{max} = \frac{\sqrt{2m}}{\hbar} (\sqrt{T} + \sqrt{T - E}). \quad (3-25)$$

3.4 Inelastic models for protons

These physics models describe interactions of slow protons (< 500 keV) and no relativistic fast protons. Ionizations and excitations contribute to energy loss in the medium. Energy lost by sub-excitation processes has been neglected. Fig. **3-7** depicts cross sections obtained by the models described above, which can be found in the Geant4 documentation and other works.

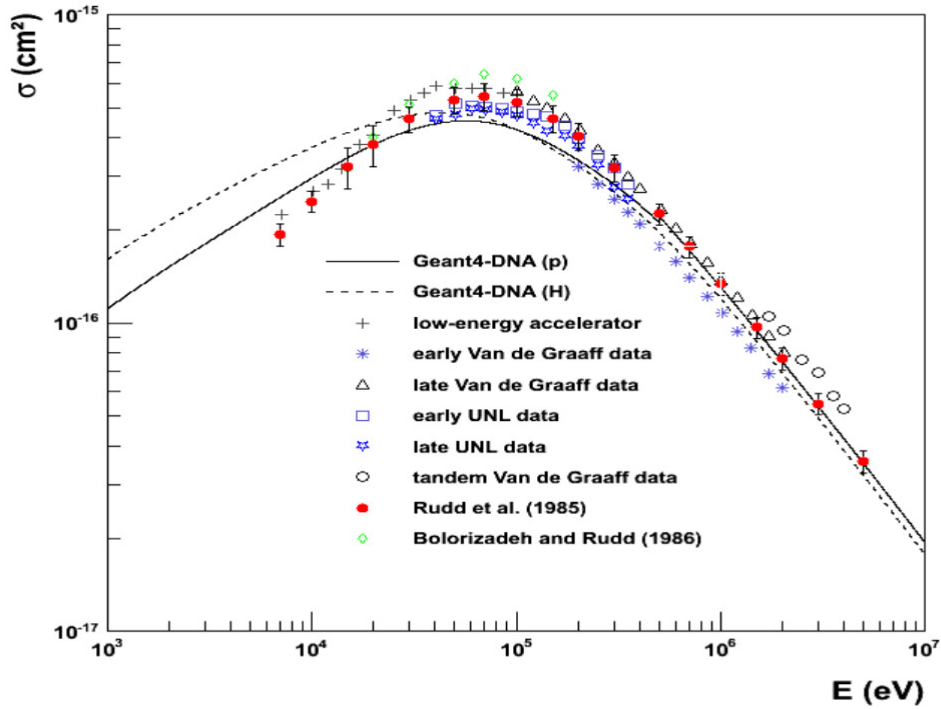


Fig. 3-7: Total cross sections of ionizations process for protons and helium atoms in water obtained from Rudd model (energies below 500 keV and from Born model (energies above 500 keV)

Ionisation

The Born theory is used for protons with energies above ~ 500 keV. For ionizations, five shells of the water molecule (4 valence and oxygen K-shell) have been taken into account. Differential ionization cross section for valence electrons of water can be obtained as follows

$$\frac{d\Sigma}{dE} = \int_{k_{min}}^{k_{max}} \frac{d^2\Sigma}{dEdK} \frac{dk}{k}, \quad (3-26)$$

where

$$K_{min} = \frac{\sqrt{2m}}{\hbar} (\sqrt{\tau} + \sqrt{\tau - E}) \quad (3-27)$$

$$K_{min} = \frac{\sqrt{2m}}{\hbar} (\sqrt{\tau} + \sqrt{\tau - E}) \quad (3-28)$$

and

$$\frac{d^2\Sigma}{dEdk} = \frac{1}{\pi a_0 T} \frac{1}{k} \eta_2(E, K) \quad (3-29)$$

is the double differential ionization cross section as a function of momentum (K) and energy (E) transfer. $T = \frac{m_e}{M} \tau$ is the reduced for of the projectiles kinetic energy $\tau = Mv^2/2$, where m_e and M are the masses of the electron and the heavy projectile, respectively. $a_0 = \hbar^2/(me^2)$ Bohr radius and $\eta_2(E, k) = Im[-1/\epsilon(E, K)]$ was described above.

Rudd's semiempirical model

Below 500 keV, the first Born approximation fails. In this interval, we have used the Rudd's semiempirical model [37] and the differential effective cross section is given by

$$\frac{d\rho}{dE} = \sum_j G_j \frac{d\rho^j}{dW_j}, \quad (3-30)$$

where E is the energy transfer, I_j is the ionization energy of the electronic shell j and $W_j = E - I_j$ is the kinetic energy of the secondary electron. G_j is a weighting factor for adjusting the result obtained by the Born approximation. In addition,

$$\frac{d\rho}{dw} = \frac{S}{B} \frac{F_1(\nu) + wF_2(\nu)}{(1+w)^3[1 + \exp\alpha(w - w_c)/\nu]} \quad (3-31)$$

with $w = W/B_j$, where B_j is a binding energy of the shell j for water vapor water and

$$F_1(\nu) = L_1(\nu) + H_1(\nu), \quad (3-32)$$

$$F_2(\nu) = \frac{L_2(\nu) + H_2(\nu)}{L_2(\nu) + H_2(\nu)}, \quad (3-33)$$

$$L_1(\nu) = \frac{C_1 \nu^{D_1}}{1 + E_1 \nu^{(D_1+4)}}, \quad (3-34)$$

$$H_1(\nu) = \frac{A_1 \ln(1 + \nu^2)}{\nu^2 + B_1/\nu^2}, \quad (3-35)$$

$$S = 4\pi a_0^2 N_j (R_y/B_j)^2, \quad (3-36)$$

where N_j is the number of electrons in shell j , and R_y is the Rydberg constant. $\nu = \frac{\tau}{B_j}$ is the projectile scaled kinetic energy and $W_c = 4\nu^2 - 2\nu - \frac{R_y}{4B_{uj}}$.

4 Method

The code used in this work was developed from the microyz example of the Geant4-DNA package, presented by the group led by Sebastien Incerti [38]. The original code was implemented to obtain microdosimetric variables such as the dose-mean lineal energy and the frequency-mean lineal energy when electrons impact on water. In this work, this code was extended so that it can be used for heavy charged particles, such as protons and α -particles. To accomplish this task, the original physical list was modified for including all the relevant physical processes that ions undergo in liquid water. In addition, a new microdosimetric variable was introduced, which is just the transfer energy. The energy transfer is defined as

$$t = \frac{\sum_V t_i}{\bar{l}} \quad (4-1)$$

where t_i is the energy transfer associated to an event (track) inside the target V and \bar{l} is the corresponding mean chord. Notice that this quantity is similar to the lineal energy but using the total energy transferred into the volume in question by the event, instead of using the imparted energy. Based on this new quantity, the dose-mean transfer energy was determined for different proton impact energies and target sizes, so the absorbed dose as had to be determined for weighting t . RBE were estimated for several target sizes and impact energies, based on both the dose-mean lineal energy and the dose-mean transfer energy.

Unlike the deposited energy, which is always confined to a sensitive site, there is also the corresponding transferred energy but a fraction of it can escape from the site. On the other hand, it is expected that the transferred energy would be related to the severity of the DNA damage. To understand the difference between the imparted energy and the transfer energy, we consider a photon and an electron entering the sensitive volume of dimensions equivalent to a cell, as shown in the Fig.4-1. Now, we can assume that an incident photon interacts through a Compton scattering, which is an important interaction for the energies used in radiotherapy. We are able to determine the probability with which the interaction takes place into the sensitive volume and the corresponding average transferred energy. However, when the interaction occurs, it is not possible to

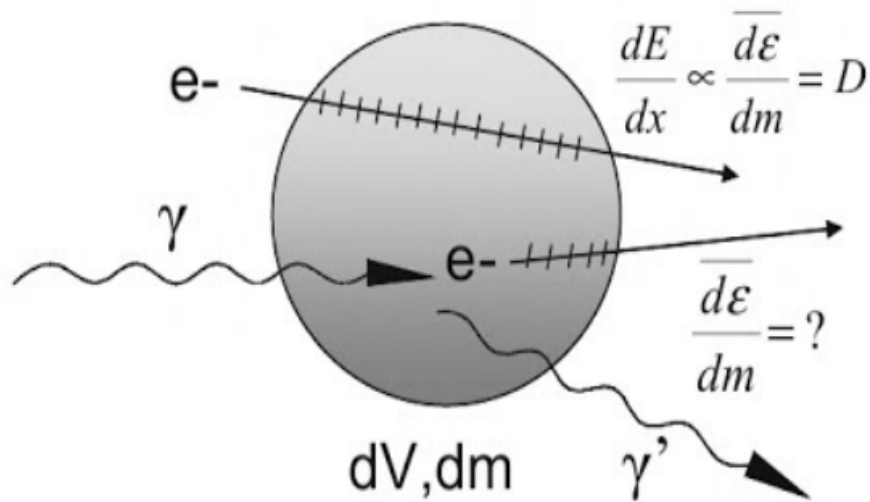


Fig. 4-1: Example of electron and photon entering the scoring volume for describing a difference between energy transfer and imparted energy .

determine with precision the energy transferred to the secondary electron nor the corresponding binding energy. This would happen with all the interactions inside the volume in question. Consequently, it is impossible to determine the imparted energy and so the specific energy. The expected value of this transferred energy per unit mass is just the macroscopic quantity kerma.

Fig.4-2 depicts the fundamental difference between these two macrodosimetric variables. From this figure we can see the kinetic energies of secondary charged particles and we can say that in this case the energy transferred is $E_T = E_1 + E_2$. However, the energy imparted would correspond to $\epsilon = E_1 + E'_2 + E_3$. In some cases, under certain conditions, these variables may be equivalent. However, as we can see, the kerma is always systematically measurable, while the absorbed dose is measurable in certain cases.

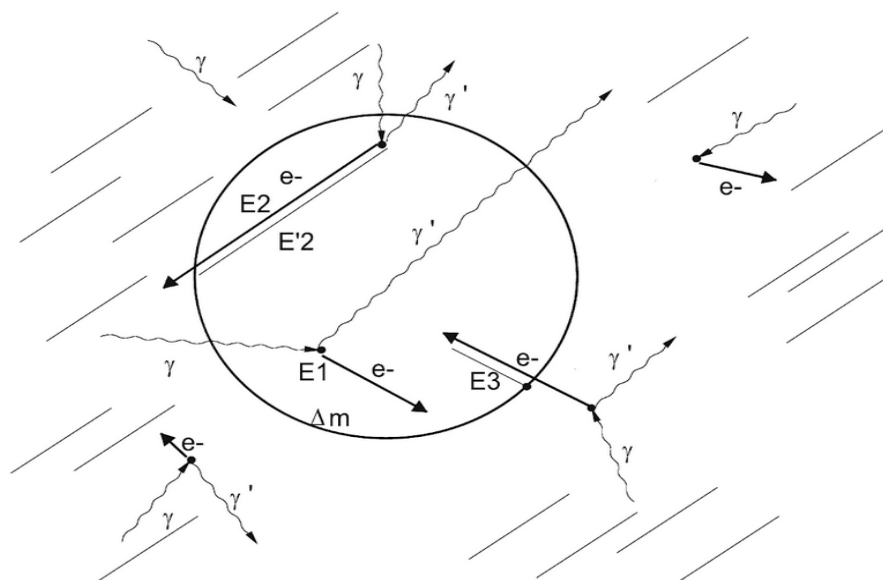


Fig. 4-2: Incident radiation impacting the scoring volume to illustrate difference between kerma and absorbed dose

4.1 The Model

The algorithm simulates the transport of a single particle through a cubic volume filled with liquid water with dimensions of a few millimeters. As particles travel into the medium, they produce energy depositions at different positions in the volume. The code is able to resolve all the depositions associated to a single primary particle, also known as track. This was done for all the primary particles and equal number of tracks were built and recorded. Later on, each track is sampled by placing microscopic spheres with sizes from 2 nm to 5 μm in a random fashion so that the lineal energy and transfer energy were determined. This model aims to emulate some structures with relevant role in radiobiology, such as the DNA double helix, the nucleosome and the 30nm chromatin fiber. After having placed the sample volume relative to the track, the corresponding energy transfers and depositions are determined, so that the lineal and transfer energies can be calculated. This process is repeated until a good statistics is achieved. This means that we can build distributions for y and t , so the dose-mean lineal energy and the dose-mean transfer energy were determined.

The model compute the number of event within to sampling sphere and determinate the value of the corresponding y and $f(y)$ for each event. A value y is calculate with the sum

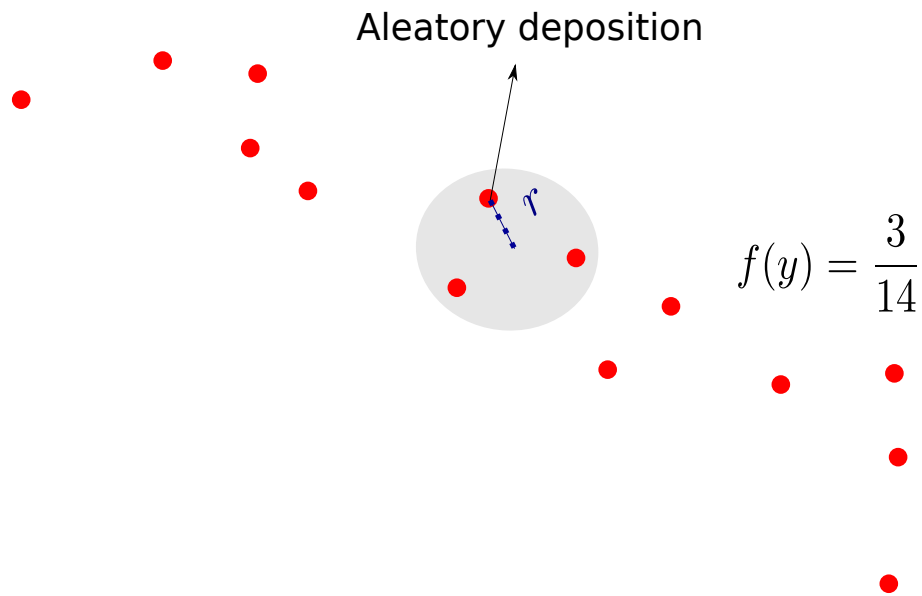


Fig. 4-3: Sampling to obtain the microdosimetric variables. In red the positions of the different depositions. One deposition is chosen randomly for each track and at a distance of not less than r the center of the sphere will do the sampling and then an $f(y)$ is defined according to the number of depositions that fall within of sphere. The total number of depositions (red points) are 14 and inside of sphere fall 3 depositions, for this reason $f(y) = \frac{3}{14}$

of deposited energy by each transfer point within of sampling sphere. The $f(y)$ value is equivalent to the number of depositions within to sampling sphere divided by the number total of transfer points of event. A scheme to trajectory of a particle, depositions of energy and sampling is shown in the Fig. 4-3. In this case a sampling sphere is located in a aleatory transfer point, in a distance no more greater to r (radius to sampling sphere). The total number of transfer points are 14 and the number of transfer point within sampling sphere is 3. In this way, with the sum of the energy deposited from these three transfer points and the chord length, the variable y is determined. In the case of the variable $f(y)$, a weight is made where the total number of depositions is related with the number of depositions within the sampling sphere, obtaining $f(y) = \frac{3}{14}$.

4.2 Organization of the user code

The *include* folder contains all the headers of the classes used. The headers correspond to all the members to the class objects, which are already defined in Geant4. These were built from the information that is available online in the Geant4 manuals. According to the needs of the particular program, some of those objects will be called in the header. Also in the headers, we define the variables that will be used in each of the codes developed for each program module. There is another folder called *src* that contains the important subroutines of the user code. These subroutines define the simulation geometry, the particle source, the physics list, and the action taken by the user in each particle's step, among others. This parts are described below, including the modification of the program to determine the new microdosimetric quantity (transfer energy) and the calculation of the RBE.

4.2.1 Description of the geometry

The detector is built in a world volume of 50μ m and in it is defined a cubic volume of half the world volume filled with water as shown in the Fig. 4-4. Inside this volume a sampling will be defined according to the shape of the biological structures that are defined inside this cubic box which will be developed in a broader way in the definition of the TrackerSD class that is in the code module where said sampling is carried out.

4.2.2 Description to physics List

In this module all the particles that can be used in the program will be defined. Among those that have been defined we have ions such as He, H, C, also fundamental particles such

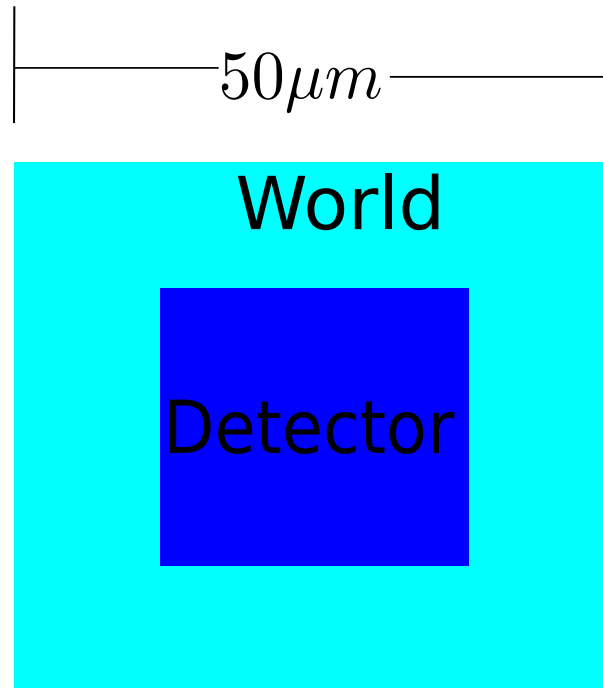


Fig. 4-4: Simulation geometry. It consist of a world with a box shape and filled with liquid water. There is also a logical smaller volume with box shape.

as protons, electrons and photons. The constructor used to models applicable to liquid water which is the main component of biological medium. These models are available in the physics constructors known as G4EmDNAPhysics in their seven options. The corresponding process classes, model classes, low energy limit applicability of models, high energy applicability of models (the kinetic energy of the particle must be less than this strict high energy limit), energy threshold (also called tracking cut) below which the incident particle is killed (stopped and the kinetic energy is locally deposited) and type of model (analytical or interpolated), and the corresponding physics constructor by electrons and protons are indicated in the Tab. 4-5 and 4-6, respectively.

4.2.3 Description of the primary source

The primary source of particles for this code is a simple model. Primary particles are isotropically emitted from the point (0,0,0), which corresponds to the center of the upper part of the box.

Interaction	Process class	Model class	Min. energy	Max. energy	Kill (1)	Type	Constructor (*)
elastic scattering	G4DNAElastic	G4DNAChampionElasticModel	7.4 eV	1 MeV	7.4 eV	interpolated	default, option2
elastic scattering	G4DNAElastic	G4DNAScreenedRutherfordElasticModel	0 eV	1 MeV	9 eV	analytical	
elastic scattering	G4DNAElastic	G4DNAUeharaScreenedRutherfordElasticModel (2)	9 eV	10 keV	10 eV	analytical	option4
elastic scattering	G4DNAElastic	G4DNACPA100ElasticModel (2)	11 eV	255 keV	11 eV	interpolated	option6
electronic excitation	G4DNAExcitation	G4DNABornExcitationModel	9 eV	1 MeV	-	interpolated	default, option2
electronic excitation	G4DNAExcitation	G4DNAEmfietzoglouExcitationModel (3)	8 eV	10 keV	-	interpolated	option4
electronic excitation	G4DNAExcitation	G4DNACPA100ExcitationModel (3)	11 eV	255 keV	-	interpolated	option6
ionisation	G4DNAIonisation	G4DNABornIonisationModel	11 eV	1 MeV	-	interpolated	default, option2
ionisation	G4DNAIonisation	G4DNAEmfietzoglouIonisationModel (4)	10 eV	10 keV	-	interpolated	option4
ionisation	G4DNAIonisation	G4DNACPA100IonisationModel (4)	11 eV	255 keV	-	interpolated	option6
vibrational excitation	G4DNAVibExcitation	G4DNASancheExcitationModel	2 eV	100 eV	-	interpolated	default, option2
attachment	G4DNAAttachment	G4DNAMeltonAttachmentModel	4 eV	13 eV	-	interpolated	default, option2

Tab. 4-5: Process included in G4DNAPhysics constructor for electrons

Interaction	Process class	Model class	Min. energy	Max. energy	Kill (5)	Type
nuclear scattering (5)	G4DNAElastic	G4DNAIonElasticModel	100 eV	1 MeV	100 eV	interpolated
electronic excitation	G4DNAExcitation	G4DNAMillerGreenExcitationModel	10 eV	500 keV	-	analytical
electronic excitation	G4DNAExcitation	G4DNABornExcitationModel	500 keV	100 MeV	-	interpolated
ionisation	G4DNAIonisation	G4DNARuddIonisationModel (G4DNARuddIonisationExtendedModel is also usable)	0 eV	500 keV	100 eV	interpolated
ionisation	G4DNAIonisation	G4DNABornIonisationModel	500 keV	100 MeV	-	interpolated
electron capture	G4DNAChargeDecrease	G4DNADingfelderChargeDecreaseModel	100 eV	100 MeV	-	analytical

Tab. 4-6: Process included in G4DNAPhysics constructor for protons

4.2.4 Description to Tracker class and sampling

This part is connected to the module of the detector construction. Once all the interactions in the homogeneous water volume box have been calculated. By means of Tracker class a Hits Collection is defined in the sensitive detector, here the momentum, deposited energy and position of each of the particles are stored. In this case the sensitive detector is a tracker type in which a hit is generated for a single step or for each tracker.

Already with the generation of the collection of the hits, we proceed to the calculation of the sampling where the second part of the geometry of the system is constructed. Here with this sampling it is assumed that a particle randomly has different energy transfer points within a volume that can be spherical or cylindrical. According to the literature presented in the first chapters, the geometric shape that best adapts to cellular organelles is the cylindrical one. Therefore, the cylindrical geometry will be implemented in addition to the part of the microyz code that will calculate the microdosimetric variables for a spherical volume.

Spherical Sampling

The sampling for the spherical geometry is done according to the model described in previous section. A deposition of a particle is chosen randomly and at the position of this deposition at a distance no greater than the radius of the sphere r_{rand} , which is defined randomly, a sampling according to the following formula is defined

$$(X_{dep} + X_{rand} + (Y_{dep} + Y_{rand})^2 + (Z_{dep} + Z_{rand})^2 < r_{sphere}^2 \quad (4-2)$$

For each of the points where the particle has made a deposition, the verification of the eqn.4-2 is performed. Which means that if it satisfy that condition, the deposition is made in a spherical volume whose center is at a distance r_{rand} .

Cylindrical sampling

In this section we will develop a methodology to implement the cylindrical sampling in the microyz code. This will allow the used of shapes similar to some DNA structures. This methodology is a modification of the TrackerSD class.

In the case of sampling a cylinder, we have to make a slightly more complex relationship. Fig.4-7 depicts the geometry of the problem, the center of that cylinder is chosen randomly

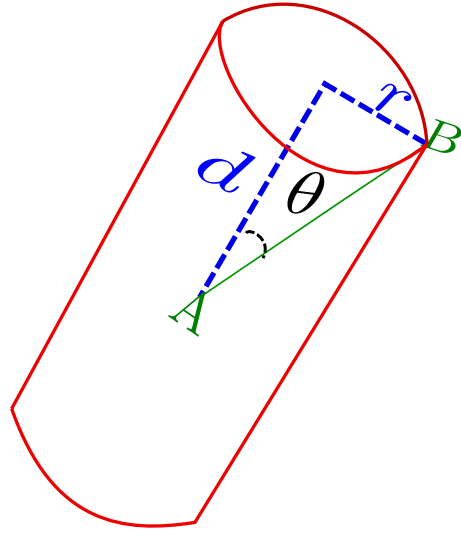


Fig. 4-7: Geometry used to find a mathematical expressions to determine if a point is inside a cylinder.

in the same way as for a sphere, with a random number r_{rand} . The cylinder has a height H equal to $2d$ and a radius equal to r . According to this figure, we can verify if the energy deposition falls inside the cylinder following this mathematical relation.

$$d = \hat{u} \cdot \overrightarrow{AB} = \overline{AB} \cos \theta \leq \frac{H}{2}$$

At the same time it must satisfy this condition

$$r = |AB|(1 - \cos \theta) \leq r_{cylinder} \quad (4-3)$$

After having found which points fall within the sampling volume, the energies deposited at these points are obtained by means of the Hits Collection method. The sum of all these energies is just the imparted energy, which is stored in a counter called *epsilon*. At the end of this process, by means of the Analysis Manager Geant4 class, the results obtained are save in a ROOT format file. These files organize the information in different columns, namely the radius of sampling volume r , number of Hits (*nofHits*), number of deposition points in each sample volume (*nbEdep*), lineal energy y , energy transfer t , and incident energy E_{inc} .

4.2.5 Determination of lineal energy and transfer energy

The determination of the linear energy y is made according to the literature, by means of the relation

$$y = \frac{\sum_i^{nbEdep} \epsilon_i}{l} \quad (4-4)$$

Tacker class has a function that allows to obtain the energy deposited at the end of each step. For which we should only call this function and include it in the Hits collection.

For the proposed new variable, which we call linear energy, we do not have to must calculate the deposited energy, in this case we need calculate the difference of kinetic energy before and after each step. For this purpose we must make a modification of the program and make use of the Step class that has as a member this calculation of kinetic energy function pre and post step, we define it inside the module of the tracker and we include it in the Collection Hits. The determination of the energy transfer is made through the following equation

According to the theory of microdosimetry, we will define a new microdosimetry variable that will be related to the transfer of energy and which we will call, t , linear energy transfer, which we will calculate according to Eqn.(4-1).

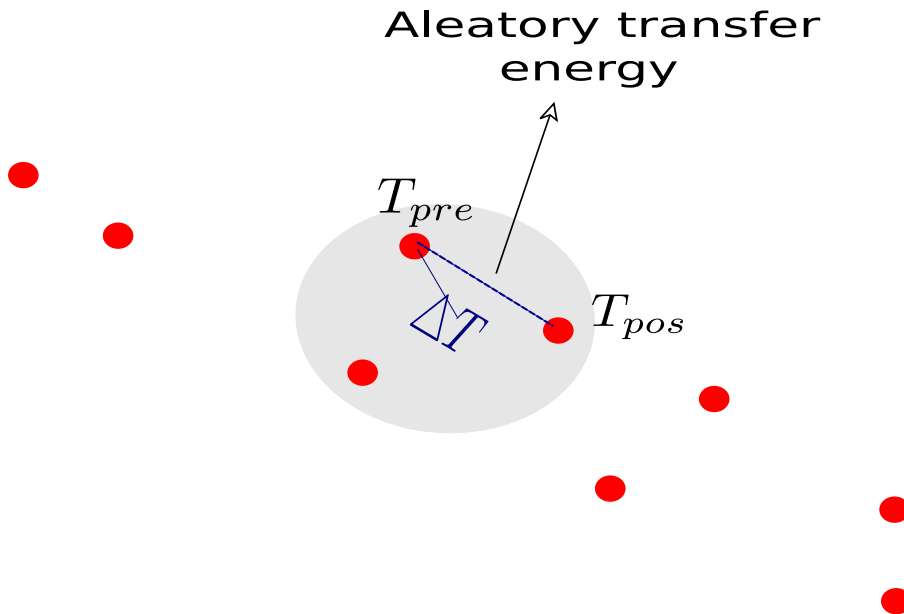


Fig. 4-8: Model to calculate transfer energy

where ϵ_t is the transfer energy and l is the chord length. The way in which this transferred energy will be calculated by similar way of the linear energy calculation, which is described in the Fig.4-8, the difference of the kinetic energy of two depositions is determinate, for which the variable will be calculated as follow

$$t = \frac{T_{pos\ step} - T_{pre\ step}}{l} \quad (4-5)$$

and it will be determined which of those interactions fall within the sphere or cylinder in a similar way to the deposited energy. From this variable we will define the dose-mean transfer energy, analogously to the dose-mean lineal energy,

$$t_d = \frac{\int z \cdot t \cdot f(t) dt}{z_f}, \quad (4-6)$$

where z is a specific energy, t is transfer energy, $f(t)$ is density distribution of variable t and z_f is frequency-mean specific energy

4.3 Determination of microdosimetric variables for reference photons

To calculate the RBE for the protons, it is necessary to determine the dose-mean lineal energy and the dose-mean transfer energy for a reference photon beam (reference quality). In this work ^{60}Co was used for reference purposes. Since microdosimetric calculations with high energy photons consumes too much time, it is common the use of the spectrum of secondary electrons produced by the incident photons. Thus, we extracted this spectrum from Ref. [39], which is shown in Fig.4-9. This spectrum was used for sampling the initial energy of the electrons that irradiate the region of interest, which was sphere with 0.5 mm radius. Now this spectrum will be the input to the program in which the physical model for Geant4-DNA of electrons will be used, which was already implemented in microyoz. For the simulation of this spectrum in Geant4 a modification is made to the class of primary generator action where the class G4GeneralParticleSource.hh will be used to give as input an electron beam whose distribution of energy goes according to the spectrum of secondary electrons.

4.3.1 Processing with ROOT

Once we have the files thrown by the program that are stored in the folder where the program is built. This program has been built to work in the multithread option, so it will throw a number of documents according to the number of cores used. The process that ROOT will perform to merge the documents thrown by geant4 and then the data obtained will be processed for the linear energy and the transferred energy to obtain the variables dose-mean linear energy and the dose-mean transfer energy, which what is done

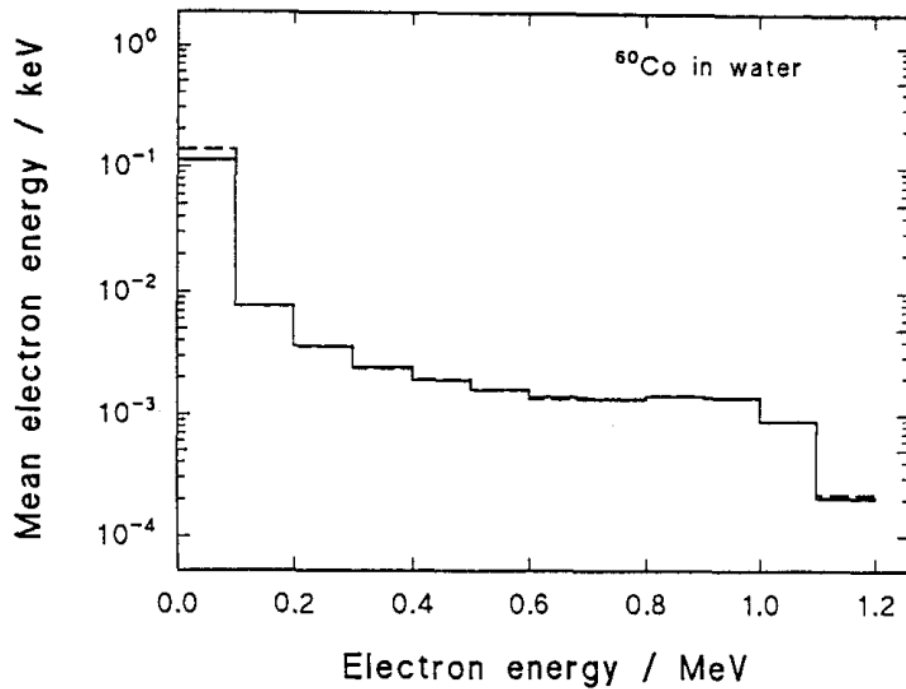


Fig. 4-9: Secondary electron spectrum ($\text{keV}^{-1}\text{photon}^{-1}$) corresponding to liquid water irradiated with ^{60}Co photons. It was used as input for determining microdosimetric variables for the reference quality.

is for each value of the frequency energy, linear energy and transfer energy is multiplied by the value corresponding to its distribution $f(y)$,

$$z_{beforeD} = \sum_{i=1}^{nEntries} \frac{nofHits}{nbEdep} * z, \quad (4-7)$$

$$y_{beforeD} = \sum_{i=1}^{nEntries} \frac{nofHits}{nbEdep} * y. \quad (4-8)$$

We also define a new variable called population that will do the following sum

$$population = \sum_{i=1}^{nEntries} \frac{nofHits}{nbEdep}, \quad (4-9)$$

Then the division of the variable $y_{beforeD}$ is made by the function $y_{beforeF}$ normalized by the function $population$, what corresponds to $y_{beforeF}/population$.

In ROOT, we also calculate the uncertainties of the variables obtained by the variance method, which is done by the following formulas. For this the first thing we will do is a calculation of error propagation, according to the formulas of y_f , where we have that the variable that has error due to the random generation of the data is $f(y)$, so it is with respect to it that the partial derivative will be made, being y a constant variable

$$\delta y_F = \sqrt{\sum_{i=1}^n \left(\frac{\partial(yf(y))}{\partial f(y)} \delta f(y)_i \right)^2} \quad (4-10)$$

$$= \sqrt{\sum_{i=1}^n (y \delta f(y)_i)^2}, \quad (4-11)$$

The uncertainty of the frequency $f(y)$ was calculated supposing that y follows a Poisson distribution

$$\delta f(y) = \sqrt{\frac{nofHits}{nbEdep}}. \quad (4-12)$$

For the case of the microdosimetric variable y_d , both the numerator and the denominator variables have an error, so the partial derivative must be made with respect to both variables and multiplied by the respective error, as it's shown in the following

$$y_D = \frac{\sum_{i=1}^n y^2 f(y)}{\sum_{i=1}^n y f(y)} = \frac{y_d}{Y_F}, \quad (4-13)$$

$$\delta y_D = \left| \frac{\partial y_D}{\partial Y_F} \right| \delta Y_F + \left| \frac{\partial Y_D}{\partial y_d} \right| \delta y_d = \frac{y_d}{Y_F} \delta Y_F + \frac{1}{Y_F} \delta y_d, \quad (4-14)$$

$$\delta y_d = \sqrt{\sum_{i=1}^n \left(\frac{\partial(y^2 f(y))}{\partial f(y)} \delta f(y)_i \right)^2} \quad (4-15)$$

$$= \sqrt{\sum_{i=1}^n (y^2 \delta f(y)_i)^2}. \quad (4-16)$$

5 Results

In this chapter we will show the development of a new sampling structure that allows us to calculate some microdosimetric quantities inside volumes with dimensions similar to those of some DNA cellular structures. This includes the proposition of a new microdosimetric quantity that is called transfer energy and the corresponding dose-mean transfer energy. This quantity is related to the stochastic quantity energy transfer. It will be compared with its analog microdosimetric quantities lineal energy and dose-mean lineal energy, which has been used along the last decades as a proxy for the relative biological effectiveness (RBE) of ionizing radiations. The capacity of both dose-mean lineal energy and dose-mean transfer energy for estimating the RBE of proton beams will be compared. To accomplish this task, both quantities will be also determined for the reference quality ^{60}Co .

5.1 Dose-mean lineal energy in different sampling structures

As mentioned in the methods section, we implemented a methodology for the calculation of the microdosimetric variable dose mean lineal energy in different sampling volumes. These calculations were made on a broad energy and for a sphere and cylinder of equivalent volumes. Where the sphere has a diameter equal to $1\ \mu\text{m}$ and the cylinder has the same length and diameter also of $1\ \mu\text{m}$. In Fig 5-1, we have the results of the simulations performed, where we found that the values of this microdosimetric variable have values very close to high energies and the greatest differences are given at low energies, not being very large. From these results we can see that structures with equivalent volumes give similar values and using a sampling as the spherical with a volume equivalent to a structure that is intended to use allows us to make a good prediction of the microdosimetric variable dose-mean lineal energy

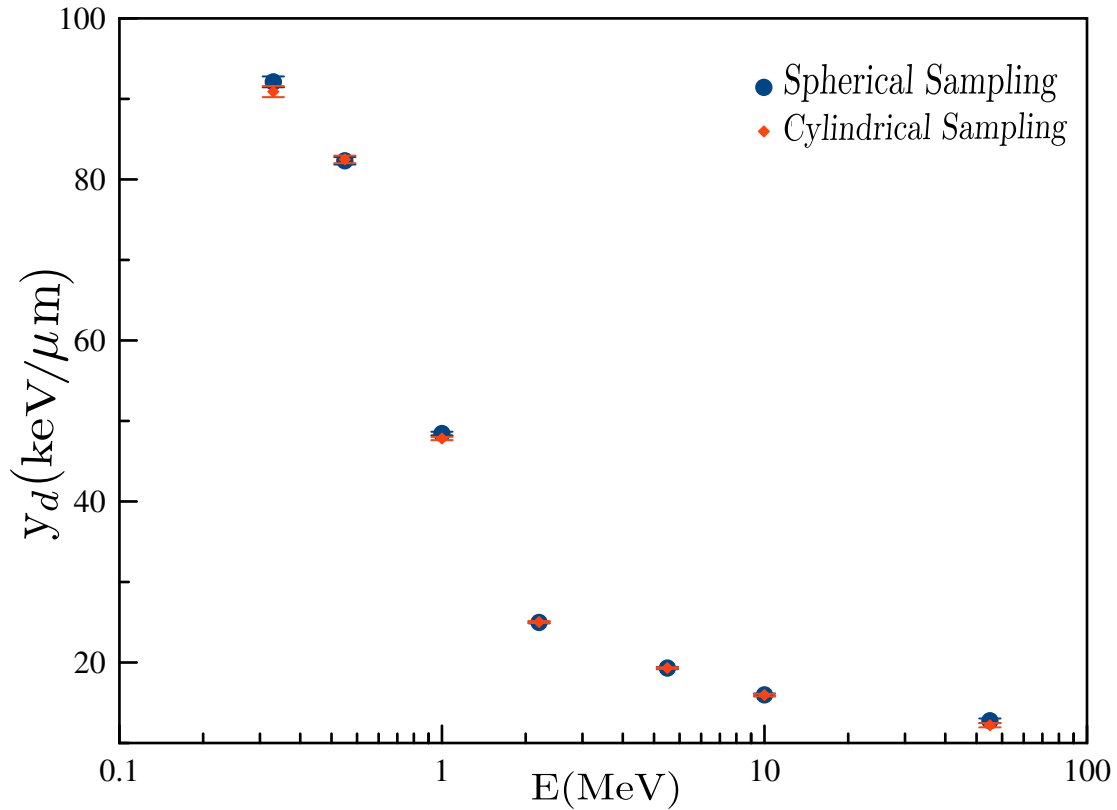


Fig. 5-1: Dose-mean lineal energy y_d obtained from sampling a spheres and cylinders of similar dimensions.

5.2 Validation of microyz for protons microdosimetry

The Monte Carlo method used by generates detailed particle trajectories in water. In that study, a segment of the trajectory was simulated. Within a segment of the path, a proton with a constant energy interacts and deposits energy along the path of the proton. The spatial deposition of energy was stored for kinetic energy greater than 12.5 eV, which was the energy of the cut off. The energy of secondary electrons below of the cutoff were absorbed locally.

The path of the segment consists of the energy of the transfer points [40]. At these points, the protons and the corresponding secondary particles lose some or all of their energy. The main tool for performing the analysis is the microdosimetric concept of proximity

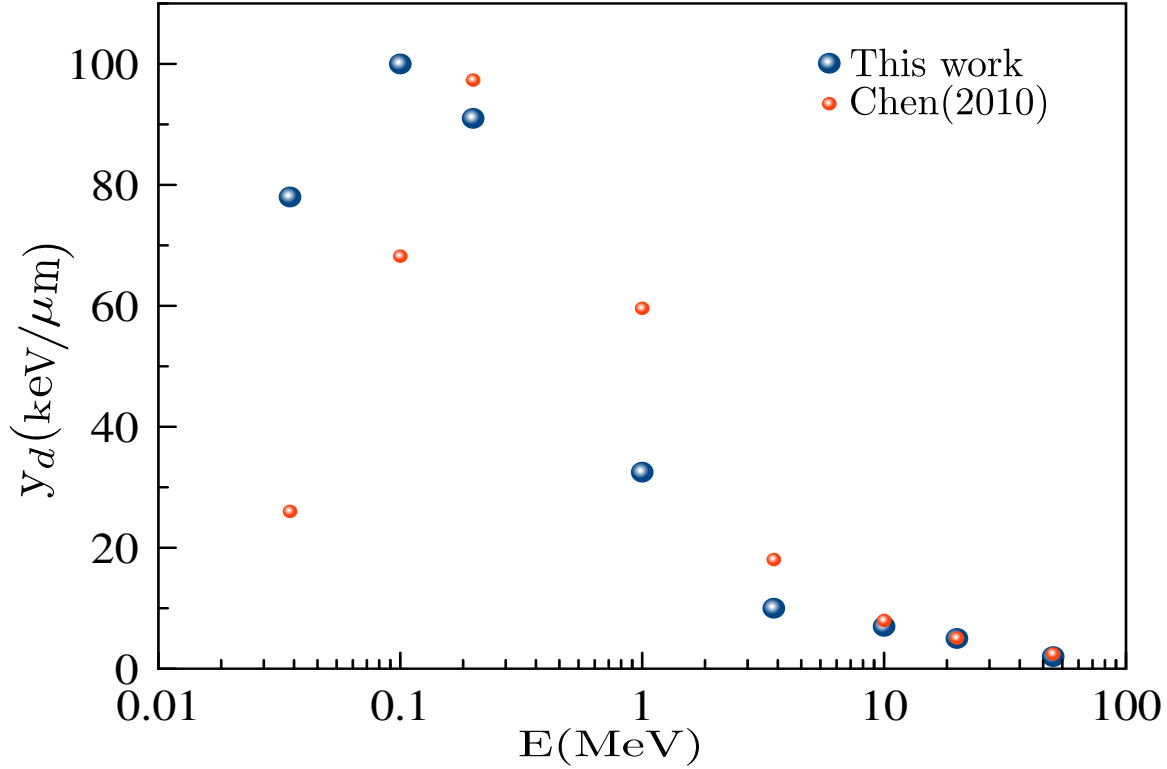


Fig. 5-2: Comparison between y_d values obtained by author with geant4 toolkit and values obtained by Chen, for a spherical region of $d = 1\mu m$

function. The proximity function is defined as a polynomial distribution. So the energy transfer points along the segment are used for the proximity function. For spherical regions, the dose-mean lineal energy can be calculated by means of the following function

$$y_D(d) = \frac{3}{2d} \int_0^d \left(1 - \frac{3x}{2d} + \frac{x^3}{2d^3}\right) t(x) dx \quad (5-1)$$

The distribution and the mean value of the microdosimetry quantities vary with the size of the volume used for sampling [41]. For technical reasons, the measurement of the distributions was simulated with different chord lengths. The sampling regions covered diameters ranging from (2-100) nm. The contribution from secondary particles to the distribution of energy was also considered, to take into account the probability density $d(y)$ and y_d for monoenergetic ions. The dose probability density was calculated by the following expression

$$d(y) = \sum_i \sum_j r_{i,j} d_{i,j}(y), \quad (5-2)$$

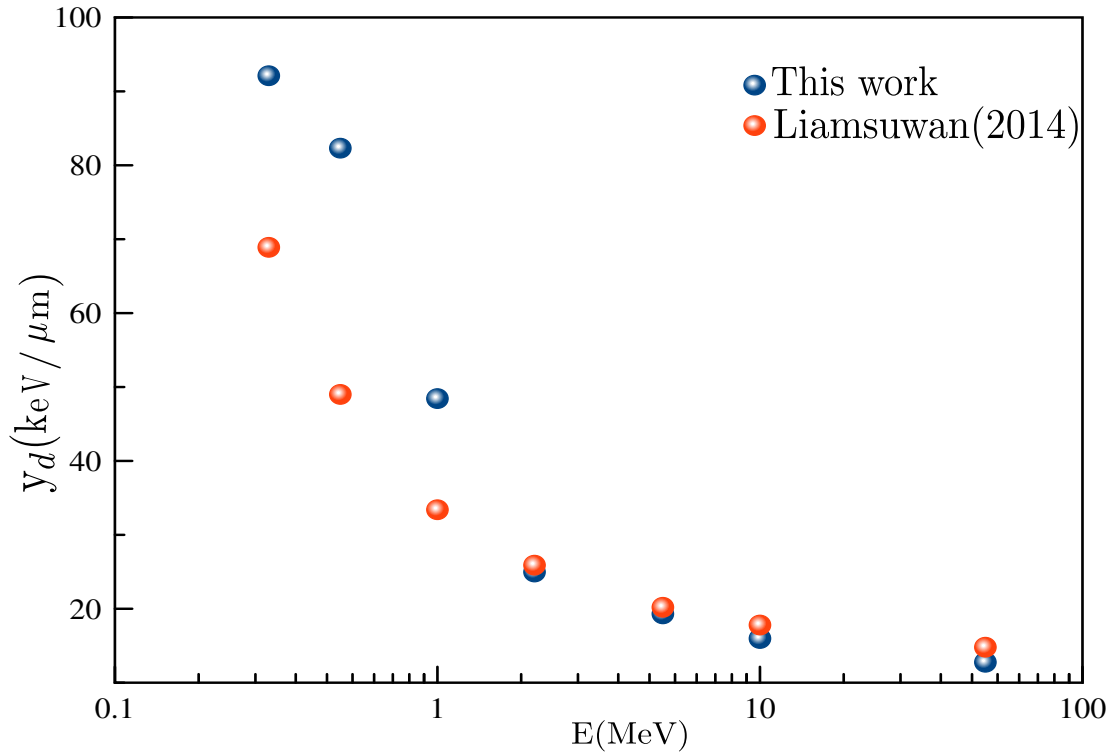


Fig. 5-3: Comparison between y_d values obtained by author with geant4 toolkit and y_d values obtained by for a cylindrical region of $d = 10\text{nm}$, equal diameters and lengths.

where $d_{i,j}(y)$ is the probability density in y for the track i and r is the relative dose fraction. The values of y_d at each depth of the Bragg curve were calculated according to

$$y_d = \int_0^{\infty} yd(y)dy. \quad (5-3)$$

5.3 Probability Density Function of microdosimetric variables

The probability density function of lineal energy is obtained from the scoring of all energy depositions occurring into the target (or probe) volume. For a selected Geant4-DNA physics constructor, tracks of incident particles (single events) are simulated one-by-one in a large volume of liquid water. Geant4 hit collections are used in order to record for each

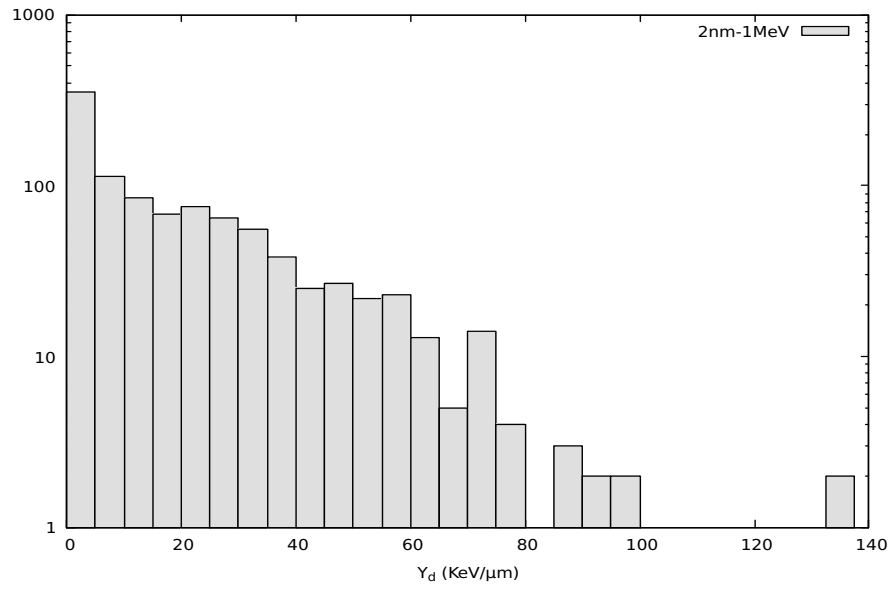


Fig. 5-4: Distribution of y_d for spherical sampling with radius 2 nm and energy equal to 1 MeV

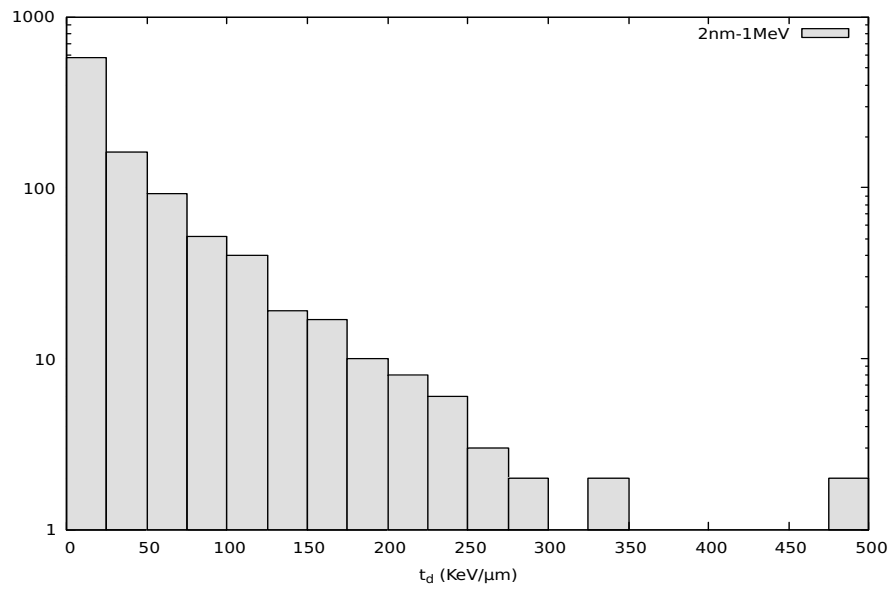


Fig. 5-5: Distribution of t_d for spherical sampling with radius 2 nm and energy equal to 1 MeV

single event all energy depositions and their location. The radius of the probe spherical

volume is chosen by the user. Once the interactions of an incident particle (single event) including all its secondary particles have all been simulated, we randomly sample one energy deposition (“hit”) and the probe volume is randomly placed at a distance from this hit less than the probe radius; all energy depositions corresponding to hits located.

5.4 Calculation of protons microdosimetric variables

As mentioned above, dose-mean lineal energy has already been widely studied and calculated by different models. In this work, it was determined based on the model proposed in the microyz example, which has already been explained in the section Methods. Once the physical list of the microyz program was adapted for the calculation of the variable dose-mean lineal energy with protons and this variable validated with results from the literature, we proceeded to calculate this variable for target sizes of 2 nm, 10 nm, 30 nm, and 5 μm , which are related to DNA and cellular structures.

For the new microdosimetric quantity (t), the Step class was implemented in the section of the TrackerSD to access the kinetic energy information between transfer points. In the previous chapter is shown how the calculation of the transferred energy is done, according to previously mentioned variables. So, the calculation of the kinetic energy between the pair of transfer points was carried out and a sampling similar to that followed for the dose-mean lineal energy was carried out. In the same way, dose-mean lineal energy was determined for target sizes of 2 nm, 10 nm, 30 nm, and 5 μm . Figs. 5-6, 5-7, 5-8 and 5-9 show the values obtained for the dose-mean lineal energy and dose-mean transfer energy for spheres with 2 nm, 10 nm, 30 nm and 5 μm . As expected, dose-mean transfer energy is greater than dose-mean lineal energy for a given target size since the energy transfer inside a volume is always greater or equal to the imparted energy. That is, a fraction of the energy transfer could escape from the site.

5.5 Photons microdosimetric variables

As previously mentioned, the two microdosimetric variables dose-mean lineal energy and the dose-mean transfer energy are required for the reference radiation. The above variables will be used to determine the RBE. The reference radiation is ^{60}Co . The microdosimetric

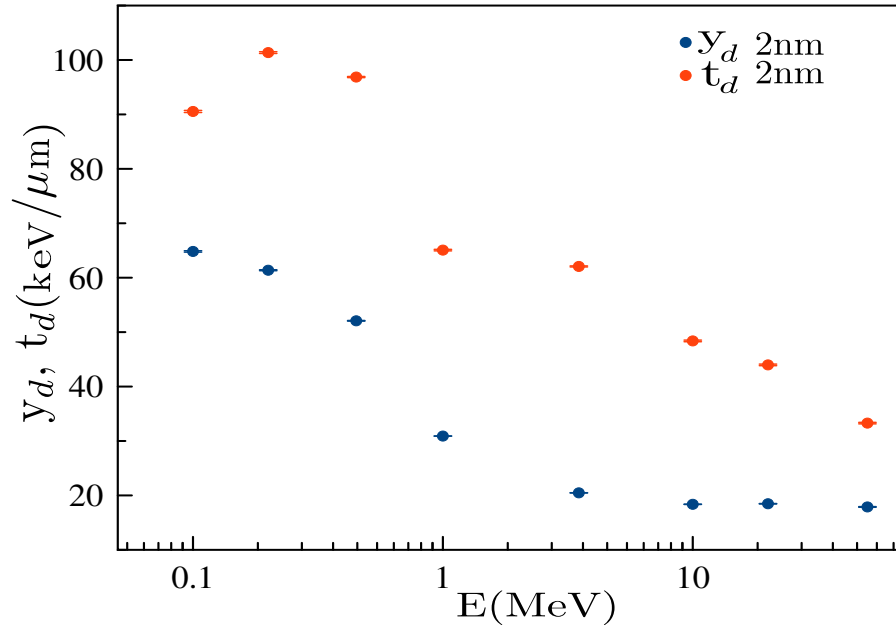


Fig. 5-6: Comparison between y_d and t_d for spherical sampling with radius 2nm

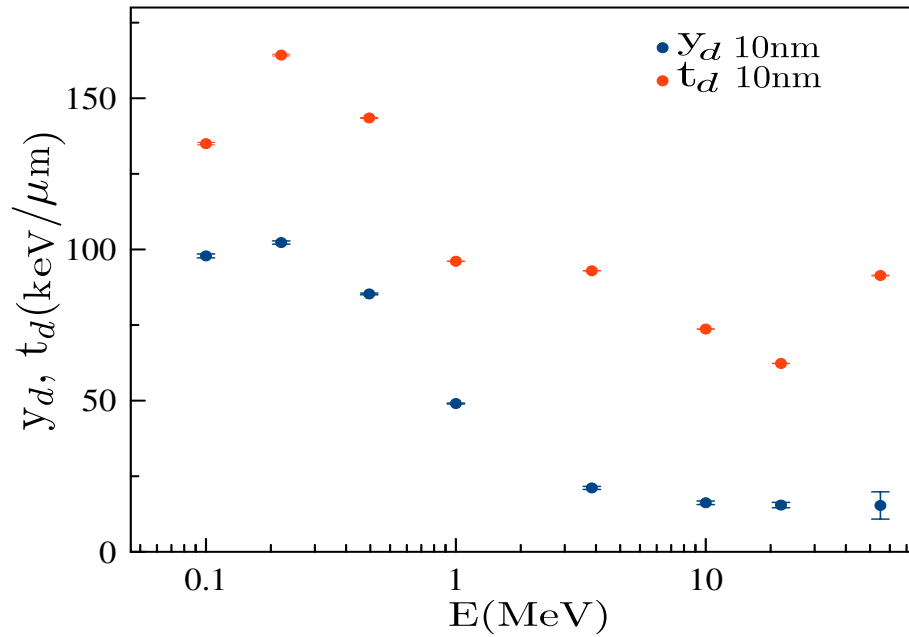


Fig. 5-7: Comparison between y_d and t_d for spherical sites with radius of 10 nm

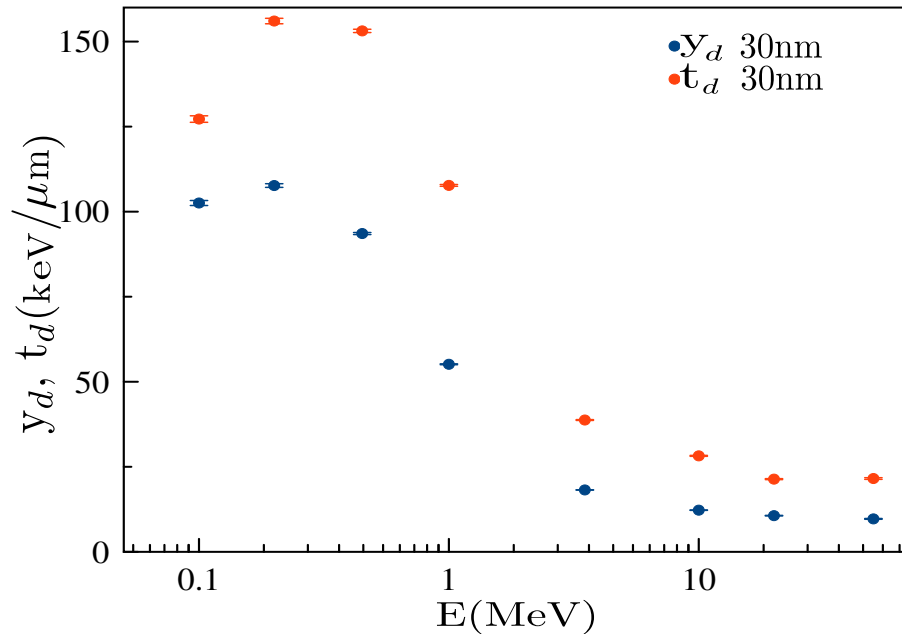


Fig. 5-8: Comparison between y_d and t_d for spherical sites with radius of 30 nm

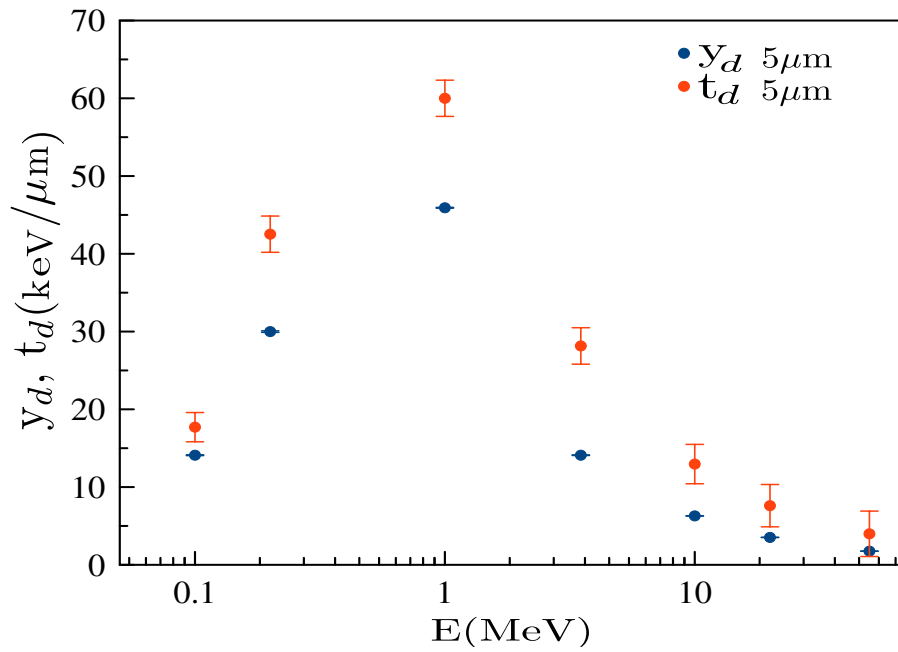


Fig. 5-9: Comparison between y_d and t_d for spherical sites with radius of 5 μm

variable of this reference radiation were determined through the secondary electron spectrum of ^{60}Co and the original microyz program, as shown in the method section. Each RBE, determined by means of y_d and t_d of protons use their respective y_d and t_d of the reference radiation, this in each radius. That is, we have a value of y_d and t_d of the reference radiation for each sampling radius. In the Tab. 5-1, we have the results for both variables in each of the sampling radios.

Diameter	y_d (keV/ μm)	t_d (keV/ μm)
2nm	17.6 ± 0.04	38.3 ± 0.1
10nm	12.36 ± 0.09	26.9 ± 0.1
30nm	8.31 ± 0.11	18.3 ± 0.2
$5\mu\text{m}$	1.04 ± 0.07	2.39 ± 0.3

Tab. 5-1: Dose-mean lineal energy y_d and dose-mean transfer energy t_d for reference radiation ^{60}Co

5.6 RBE calculation

RBE quantifies how efficient per unit absorbed dose is a radiation quality to induce some biological effect. In hadrontherapy, RBE is described in terms of absorbed dose and this is known as the RBE-weighted absorbed dose. In proton therapy, a constant value of the RBE is used along the Spread Out Bragg Peak region, while for carbon ions there is a remarkable dependence of the RBE with LET in this region.

For the investigation on the response to ion beams in the PIDE, RBE values were calculated from the LQ parameters. In this database was combined a variety of experimental results of ion irradiation experiments with in vitro cell lines including the early experiments from Berkeley [42, 43], the huge datasets of studies from Japan [44, 45] and the experiments carried out in Europe. After a thorough literature survey, in this work was introduced some restriction for the selection of the publications included in the data ensemble. One of these restrictions was included publications for which the LQ parameters for the response to photons as reference radiation were available or derivable. Note that these may deviate from directly measured RBE values.

In investigations on tissue response to different ion doses, the determination of the RBE is commonly based on the LQ model. The different doses used in the experiments can

generate deviations in the RBE values. In particular, in the high dose region the LQ model has been questioned. To investigate the impact of the LET on radiosensitivity, the RBE was plotted versus LET for different particle species. The analysis performed by Friedrich et al. was restricted to values the RBE_α and RBE_{10} corresponding to the initial slope (upper row) and 10% survival level (lower row). The cells used for the analysis were classified into high and low photons α/β , which are either above or below 4 Gy, respectively.

In most microdosimetry applications, particularly in the field of radiotherapy with neutrons, a simple way to describe the quality of radiation is the introduction of an empirical weighting function. In this work, the estimation of RBE was made by means of a simple relation in terms of some microdosimetry quantities found for protons and photons. The relation used is an approximation and does not take into account any biological endpoint. The intention of this approach is to have a preliminary estimation of the RBE based only on physical quantities, linked to the track structure of the radiation. We expect that this approach allows to make a comparison between the well-known dose-mean lineal energy and the one proposed in this work: the dose-mean transfer energy. The reason why we decided to use an approximation of the RBE without taking into account any biological endpoint is the absence of experimental models for the calculation of the RBE with such a the new quantity. The RBE for the case of dose-mean linear energy is

$$RBE = \frac{y_{d\text{proton}}}{y_{d\text{photon}}}. \quad (5-4)$$

We have followed an analog approach for the case of the dose-mean transfer energy:

$$RBE = \frac{t_{d\text{proton}}}{t_{d\text{photon}}}. \quad (5-5)$$

Figs. **5-10**, **5-11**, **5-12**, and **5-13** show the RBE determined from the two microdosimetric quantities in question. These calculations were made for different target sizes, namely 3nm, 10nm, 30nm, and 5 μ m. It can be observed in Tab. **5-1** that t_d is greater than y_d for the reference radiation. In fact, t_d is more than twice as large as y_d . This is why the RBEs obtained from t_d are lower than those calculated using y_d , despite that t_d is always greater than y_d . The reference radiation, ^{60}Co , produces very energetic electrons that can transfer higher energies to other electrons when compared to heavy charged particles. Furthermore, these energetic electrons have greater chances for escaping from the target. Thus, the average energy transfer may be higher than the average energy deposit per event. The latter quantity is the one used for determining the lineal energy.

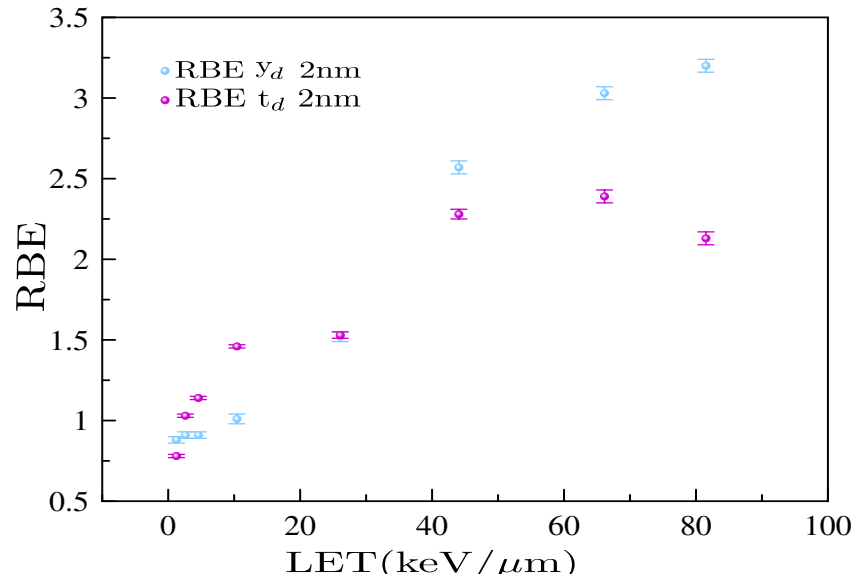


Fig. 5-10: RBE determined for a spherical sampling volume with 2 nm radius for both microdosimetric quantities.

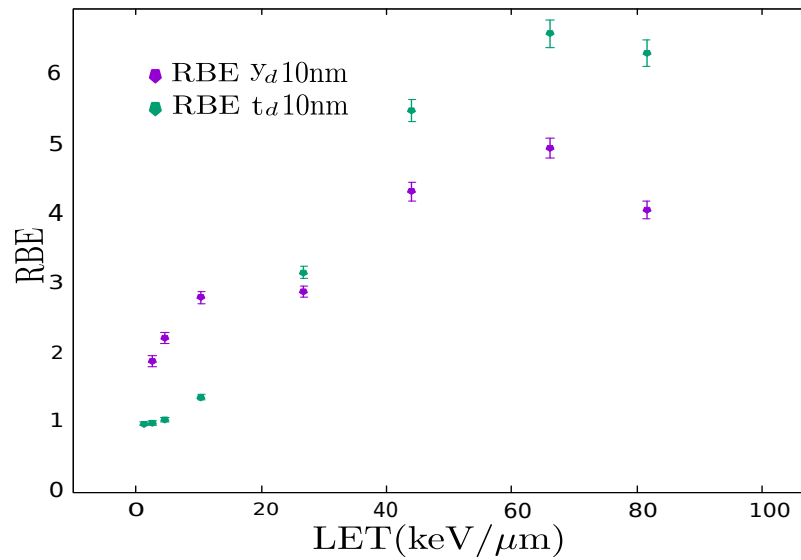


Fig. 5-11: RBE determined for spherical a sampling volume with 10 nm radius for both microdosimetric quantities.

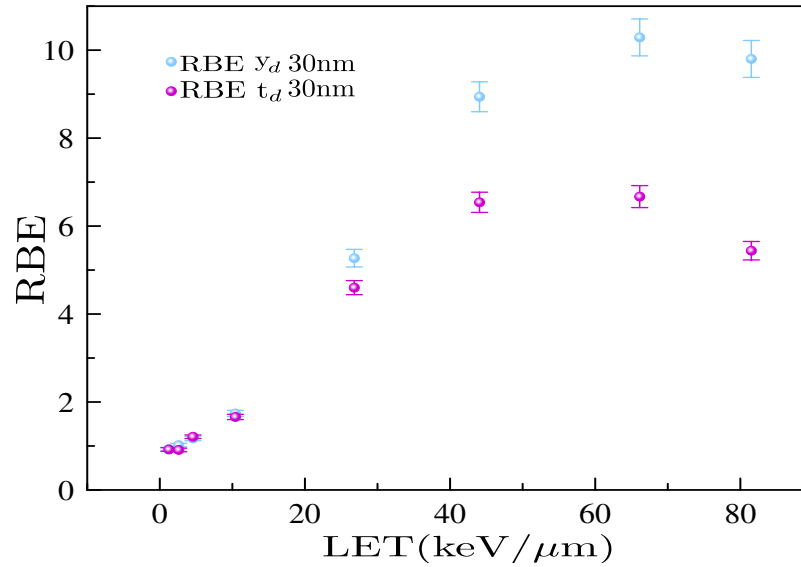


Fig. 5-12: RBE determined for a spherical sampling volume with 30 nm radius for both microdosimetric quantities.

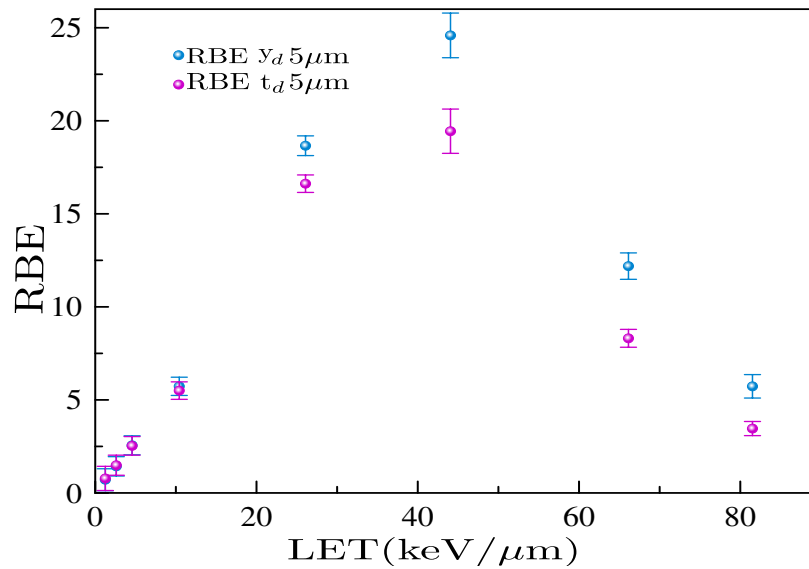


Fig. 5-13: RBE determined for a spherical sampling volume with 5 μm radius for both microdosimetric quantities.

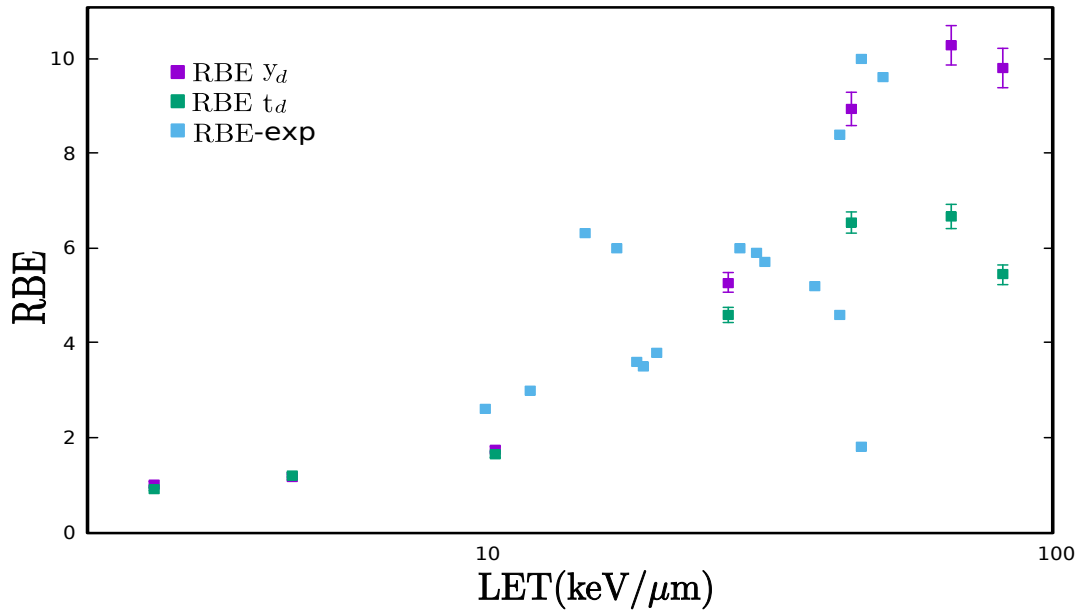


Fig. 5-14: Graph obtained for comparison of RBEs obtained by author with diameter 30nm and the data values of experimental measurements of RBE

The graphs obtained by Eqns. (5-4) and (5-5), taking into account each of the two proposed microdosimetric quantities, show that the value of transferred energy is always greater than the lineal energy, as expected because a fraction of the transfer energy can escape from the target volume. From these results we find that the transfer energy is greater than the lineal energy. When we calculate RBE, the difference between transfer energy and lineal energy for photons and protons are somehow compensated. The RBE obtained from the microdosimetry quantity associated to the transfer energy is lower than that obtained from the lineal energy. Also we note that while the sampling radius increases, the RBEs calculated for both quantities become closer. A comparison was made between the experimental data for RBE_α extracted from Ref. [23] and our results for the 30 nm diameter cases, which are shown in Fig. (5-14).

The experimental results shows that it is still difficult to make a consensus on the RBE values in *in vitro* studies, mainly due to the dispersion of their results. For RBE_α , the experimental RBE values are closer to our results obtained for the radius of 30nm, specially for the RBE obtained from the dose-mean lineal energy. From these results we find a good correspondence of the RBE values of new microdosimetry variable proposed and the older microdosimetric variable with experimental data of RBE.

6 Conclusions

This thesis establishes a methodology for using the Monte Carlo track structure code Geant4 to quantify the old quantity dose-mean lineal energy and the new one, dose-mean transfer energy. This was done for protons and ^{60}Co photons, in order to estimate proton RBE using both quantities. Such quantities were determined for different volume shapes and sizes to find out which better correlates to experimental RBE. The code used here is based on the microyz example of the Geant4 package. The dimensions of the sampling sites were chosen similar to some DNA and cellular structures.

The results presented in this thesis show the validation of the code with other microdosimetric models for the determination of y_d . From this validation, it was found that the application of the physical constructors used in Geant4 for heavy particles allow the estimation of such a variable with very good agreement, both for high and low proton impact energies.

The code was extended for being used with cylindrical sampling volumes, since some DNA structures have this shape. The largest discrepancies for the dose-mean lineal energy were found for low energies. For high energies, difference are not higher than 5%. Discrepancies can be attributed to different physical models used by the corresponding MC codes, although the shape of the sampling volumes can influence the results even when they have the same mean cord.

For each shape, sphere and cylinder, a Geant4 simulation code was developed for reporting the deposited and the transferred energy per single interaction. Proton beams with the energy ranging from 10 keV to 50 MeV were used as primary particles, besides photon from ^{60}Co . From the simulation, the lineal energy and transfer energy distributions were built. The results show that the smaller the site the larger the difference between these two quantities. This could expected because more energy escape from smaller volumes when compared to the total transferred energy. For the largest sampling volume, these two quantities show reasonable agreement, since electronic equilibrium may be achieved in this situation.

It was also found that the dose-mean transfer energy is more sensitive to the shape of the sampling volume than the dose-mean lineal energy.

In the last part of this work, the RBE was calculated using both the dose-mean lineal

energy and the new quantity, dose-mean transfer energy. ^{60}Co photons were used as the reference quality. We found that the dose-mean linear energy and the dose-mean transfer energy resembles the experimental RBE vs. LET. Thus, the new quantity could be a good predictor of the RBE, in the same way than the old one.

Modern particle radiotherapy demands more research in the field of microdosimetry and Radiobiology. It is expected that this work can be extended so that the viability of the dose-mean transfer energy may be finally confirmed as a good microdosimetric estimator of RBE.

Bibliography

- [1] N. J. Marlies Pasler, Victor Hernandez and C. H. Clark, “Novel methodologies for dosimetry audits: Adapting to advanced radiotherapy techniques,” *Physics and Imaging in Radiation Oncology*, vol. 5, pp. 76–84, 2018.
- [2] D. Frankenberg, “Repair of dna double-strand breaks and its effect on rbe,” *Adv. Space Res.*, vol. 14, pp. (10)235–(10)248, 1994.
- [3] L. B. Rodolphe Antoni, *Applied Physics of External Radiation Exposure: Dosimetry and Radiation*. Switzerland: Longman, 2017.
- [4] N. A. A. M. e. a. Paganetti, H., “Relative biological effectiveness (rbe) values for proton beam therapy,” *International Journal of Radiation Oncology Biology Physics*, vol. 53(2), p. 407–421, 2002.
- [5] K.-W. W. Scholz M, Kellerer A M and K. G., “Computation of cell survival in heavy ion beams for therapy,” *Radiat. Environ. Biophys.*, vol. 36, pp. 59–66, 1997.
- [6] H. RB, “A microdosimetric-kinetic model of cell death from exposure to ionizing radiation of any let, with experimental and clinical applications,” *Int J Radiat Biol.*, vol. 69:7, pp. 39–55, 1996.
- [7] S. M and K. G., “Track structure and the calculation of biological effects of heavy charged particles,” *Radiat. Environ. Biophys.*, vol. 18, pp. 5–14, 1996.
- [8] H. H. Rossi, “The role of microdosimetry in radiobiology,” *Radiation and Environmental Biophysics*, vol. 17, pp. 29–40, 1979.
- [9] H. P. M Dingfelder, M. Inokuti, “Inelastic-collision cross section of liquid water for interactions of energetic protons,” *Radiat. Phys. Chem.*, vol. 59, pp. 255–275, 2000.
- [10] H. P. M Dingfelder, L.H. Hantke, “Electron inelastic scattering cross section in liquid water,” *Radiat. Phys. Chem.*, vol. 53, pp. 1–18, 1998.
- [11] H. A. Bethe, “Molière’s theory of multiple scattering,” *Radiation and Environmental Biophysics*, vol. 17, p. 1256, 1979.

- [12] M. L. Grevillot, "Monte carlo simulation of active scanning proton therapy system with gate/geant4," 2011.
- [13] A. J. Wroe, J. D. Slater, and J. M. Slater, "The physics of protons for patient treatment," 2012.
- [14] Francis, "Simulations monte carlo et étude microdosimétrique pour des irradiations cellulaires à faibles doses en neutrons de 14 mev," 26 Octobre 2007.
- [15] J. Kiefer, "Cellular and subcellular effects of very heavy ions," *J. RADIAT. BIOL.*, vol. 48, pp. 873–892, 1985.
- [16] G. A. Cruz, *Microdosimetry: Principles and applications*, vol. 21. March–April 2016.
- [17] D. C. A. M. Kellerer, "Concepts of microdosimetry," *Radiation and Environmental Biophysics*, vol. 12, pp. 205–216, 1975.
- [18] D. J. Thomas, "Icru report 85: fundamental quantities and units for ionizing radiation," *Radiation and Environmental Biophysics*, vol. 150, pp. 550–552, 2012.
- [19] R. HH, *Microscopic energy distribution in irradiated matter*. New York: Academic Press, 1986.
- [20] M. Z. Harald H. Rossi, *Microdosimetry and Its Applications*. USA: Springer, 1996.
- [21] K. Chadwick and H. Leenhouts, *The molecular theory of radiation biology*. Berlin: Springer-Verlag, 1981.
- [22] M. D. Alexander Helm, Walter Tinganelli, "Advances in radiation biology of particle irradiation," *Prog Tumor Res. Basel, Karger*, vol. 44, p. 436–439, 2018.
- [23] T. E. M. D. Thomas Friedrich, Uwe Scholz and M. Scholz, "Systematic analysis of rbe and related quantities using a database of cell survival experiments with ion beam irradiation," *Adv. Space Res.*, vol. 54, p. 494–514, 2013.
- [24] C. P. Karger and P. Peschke, "Rbe and related modeling in carbon-ion therapy," *Phys. Med. Biol.*, vol. 63, 2018.
- [25] F. J. F, "The linear-quadratic formula and progress in fractionated radiotherapy br," *J. Radiol.*, vol. 62, 679-9.
- [26] F. K. I. H. E.-K. K. Kanai T, Furusawa Y and O. H, "Irradiation of mixed beam and design of spread-out bragg peak for heavy-ion radiotherapy," *Radiat. Res.*, vol. 147, 78-85.

-
- [27] M. B. C. R.-L. Djamel Dabli, Gerard Montarou, “Rbe modelization: Present status and future prospects,” *Phys. Med. Biol.*, vol. 63, 2018.
- [28] F. V. Joao Seco, *Monte Carlo Techniques in Radiation Therapy*. Taylor and Francis Group, 2013.
- [29] J. L. Devore, *Probabilidad y Estadística para Ingenierías y Ciencias*. 2008.
- [30] A. F. Bielajew, *Fundamentals of the Monte Carlo method for neutral and charged particle transport*. USA: The University of Michigan, 1998.
- [31] F. G. Garzon., ed., *Tome la mejor decisión experimentando previamente sus consecuencias*. España: OmniaScience, 2017.
- [32] L. B. Castañeda, *Probabilidad*. Universidad Nacional de Colombia, 2004.
- [33] I. Kawrakow, “Accurate condensed history monte carlo simulation of electron transport i.egsnrc, the new egs4 version,” *Med. Phys.*, pp. 485–498, 2000.
- [34] C. M. Terracciano, “Analysis and interpretation of carbon ion fragmentation in the bragg peak energy range.,” 2015.
- [35] G. P. R. Manual, “Geant4 collaboration,” *Physics Reference Manual*, pp. 1–18, 2018.
- [36] M. T. Coghill, “Radiobiological modeling using track structure analysis,” 2012.
- [37] M.E.Rudd, “User-friendly model for energy distribution of electron from proton or electron collision,” *Nucl. Tracks Radiat.Meas*, vol. 16, pp. 213–218, 1989.
- [38] V. I. M. C. B.-e. a. I. Kyriakou, D. Emfietzoglou, “Microdosimetry of electrons in liquid water using the low-energy models of geant4,” *Journal of Applied Physics*, vol. 122, 2017.
- [39] S. U. . H. Nikjoo, “Energy spectra of secondary electrons in water vapour,” *Radial Environ Biophys*, vol. 35, pp. 153–157, 1996.
- [40] J. Chen, “Microdosimetric characteristics of proton beams from 50 kev to 200 mev,” *Radiation Protection Dosimetry*, vol. 143, p. 436–439, 2011.
- [41] L. L. S. U. Thiansin Liamsuwan, Martha Hultqvist and H. Nikjoo, “Microdosimetry of proton and carbon ions,” *Medical Physics*, vol. 41, 2014.

-
- [42] S. K. e. a. Chapman JD, Blakely EA, “Radiation bio-physical studies with mammalian cells and a modulated carbon ion beam,” *Radiat Oncol Biol Phys*, vol. 3:97-102, 1977.
- [43] Y. T. e. a. Blakely EA, Tobias CA, “Inactivation of human kidney cells by high-energy monoenergetic heavy-ion beams,” *Radiat Res*, vol. 80:122-60, 1979.
- [44] D. M. Furusawa Y, Aoki M, “Simultaneous exposure of mammalian cells to heavy ions and x-rays,” *Adv Space Res*, vol. 30:877–84, 2002.
- [45] O. I. e. a. Takahashi A, Ohnishi K, “p53–dependent thermal enhancement of cellular sensitivity in human squamous cell carcinoma in relation to let,” *Int J Radiat Biol*, vol. 77:1043–51, 2001.